Geological Magazine

www.cambridge.org/geo

U–Pb ages of Miocene near-trench granitic rocks of the Southwest Japan arc: implications for magmatism related to hot subduction

Hironao Shinjoe[1], Yuji Orihashi[2] and Ryo Anma[3]

[1]Tokyo Keizai University, 1-7-34 Minami-cho Kokubunji, Tokyo 185-0021, Japan; [2]Department of Earth and Environmental Sciences, Faculty of Science and Technology, Hirosaki University, 3 Bunkyo-cho, Hirosaki, Amori 036-8561, Japan and [3]Graduate School of Technology, Industrial and Social Sciences, Tokushima University, 2-1 Minami-josanjima, Tokushima 770-8506, Japan

Original Article

Cite this article: Shinjoe H, Orihashi Y, and Anma R (2021) U–Pb ages of Miocene near-trench granitic rocks of the Southwest Japan arc: implications for magmatism related to hot subduction. *Geological Magazine* **158**: 47–71. https://doi.org/10.1017/S0016756819000785

Received: 18 October 2018
Revised: 28 May 2019
Accepted: 30 May 2019
First published online: 7 November 2019

Keywords:
zircon; Philippine Sea plate; Japan Sea; felsic rocks

Author for correspondence:
Hironao Shinjoe, Email: shinjoe@tku.ac.jp

Abstract

We present a new dataset of zircon U–Pb ages that document igneous activity in the SW Japan arc during middle Miocene time and discuss its relationship with the opening of the Japan Sea, Philippine Sea plate migration, and subduction of the young hot lithosphere of the Shikoku Basin. Precursory magmatism, characterized by dike and stock intrusions, started *c.* 15.6 Ma in both Kyushu and the Kii Peninsula. Most plutonism occurred between 15.5 and 13.5 Ma in an area 600 km long and 150 km wide. No along-arc trend was recognized in the U–Pb ages of igneous activity near the trench. Our data indicate that all near-trench middle Miocene igneous activity occurred immediately after the opening of the Japan Sea ceased, i.e. after 16 Ma, implying that melt extraction and the emplacement of granites in the near-trench region had some influence on the back-arc opening. Our data also imply that the trench–trench–trench-type triple junction between the Japan arc and the Izu–Bonin–Mariana arc must have reached the east side of the Kii Peninsula by 15.6 Ma. The wide distribution of contemporaneous magmatic activity along the arc requires a trench-parallel heat source, such as the subduction of a trench-parallel ridge or a young and highly segmented ridge–fracture zone system in addition to the hot wedge mantle condition related to the opening of Japan Sea.

1. Introduction

In the SW Japan arc, igneous rocks of Miocene age are distributed in a belt 800 km long and 150 km wide (Figs 1, 2). During middle Miocene time, intensive magmatism took place in a region closer to the Nankai Trench than the Quaternary volcanic front, just behind fore-arc basins that are filled with middle to late Miocene sediments (Fig. 2). Such near-trench magmatism cannot be explained by the conventional model of magma generation in island arc settings (e.g. Tatsumi, 1989). Instead, it is commonly thought to form as a consequence of ridge subduction (DeLong *et al.* 1979; Iwamori, 2000; Kimura *et al.* 2005). The 'blowtorch effect' related to the rise of asthenospheric mantle through slab windows (DeLong *et al.* 1979) may also have enhanced slab melting by the subduction of a young and hot oceanic plate (Defant & Drummond, 1990).

The origin of middle Miocene magmatism in the SW Japan arc is usually ascribed to the subduction of hot lithosphere of the Shikoku Basin, the product of a spreading ridge in the Philippine Sea plate, because the magmatism is almost coeval with the initiation of Philippine Sea plate subduction, immediately after the opening of the Japan Sea and clockwise rotation of SW Japan (Fig. 1) (Kimura *et al.* 2005; Tatsumi, 2006). Because spreading of the Shikoku Basin continued until *c.* 15 Ma (Okino *et al.* 1999), subduction of this spreading ridge and fracture zone system is thought to have taken place at the same time as the magmatism (Maruyama, 1997; Kimura *et al.* 2005). This tectonic interpretation largely depends on the assumption that the proto-Izu–Bonin–Mariana (IBM) arc had arrived near its present position before magmatism began (Seno & Maruyama, 1984).

An alternative explanation is that the near-trench magmatism occurred as the trench–trench–trench (TTT)-type triple junction of the Pacific, Philippine Sea and Eurasia plates migrated eastward during the opening of the Shikoku Basin (Marshak & Karig, 1977). Some plate reconstruction models that emphasize clockwise rotation of the Philippine Sea plate during Miocene time based on the palaeomagnetic evidence favour this model (Hall *et al.* 1995; Hall, 2002; Sdrolias *et al.* 2004). Clift *et al.* (2013) provided independent evidence to support the triple-junction migration model: middle Miocene sediments in the accretionary prism of the Nankai Trough contain zircon crystals with wide age ranges, which implies that they were supplied directly from the Yangtze River to the Shikoku Basin. Thus, at that time the Kyushu–Palau

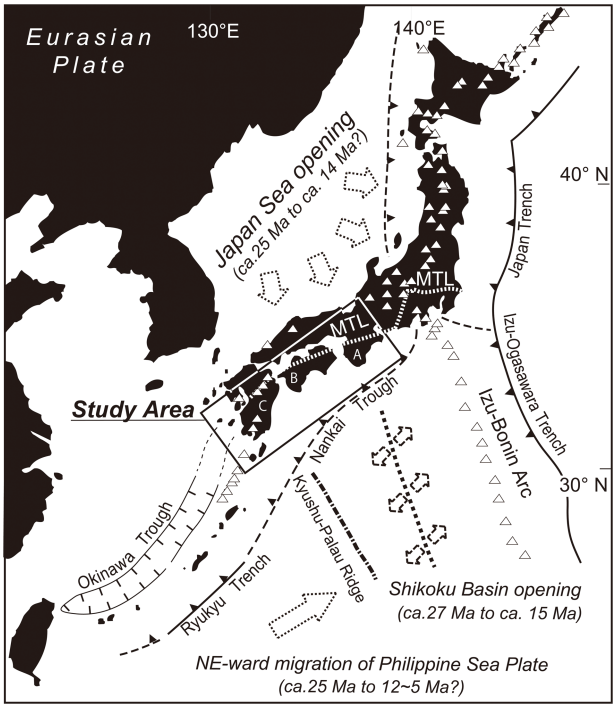

Fig. 1. Index map showing the tectonic setting of the Japanese Islands and the location of the SW Japan arc (rectangle). Also indicated are Miocene tectonic events including the rapid clockwise rotation of the SW Japan arc related to the opening of the Japan Sea and the clockwise rotation of the Philippine Sea plate. An extinct spreading ridge on the Philippine Sea plate that formed the Shikoku Basin is indicated with dashed lines. Open triangles are Quaternary volcanoes. Localities in the study area: A, Kii Peninsula; B, western Shikoku; C, Kyushu; MTL, Median Tectonic Line.

Ridge to the west of the Shikoku Basin was not a topographical barrier that prevented direct inflow of sediments through the East China Sea. Kimura *et al.* (2014) interpreted the eastward migration of magmatism in middle Miocene time within the framework of the triple-junction migration model, suggesting that the migration was related to the movement of the proto-IBM arc. However, because of most of their K–Ar ages with a low analytical precision, more precise and consistent age data were needed to trace the development of the SW Japan arc in detail.

In this paper, we present newly obtained zircon U–Pb ages of near-trench felsic rocks in the SW Japan arc. These data were obtained from an elongated area parallel to the trench more than 100 km across and 600 km long. Although Miocene magmatism extends from the Ryukyu arc in the south to the Honshu–IBM arc collision zone, we concentrated on the region between the island of Kyushu and the Kii Peninsula, where the evidence of Miocene magmatism has not been disturbed by later magmatism related to the IBM arc collision.

2. Geological background

2.a. Outline of geology

The SW Japan arc is divided along the Median Tectonic Line into the Outer Zone, on the south side nearer to the trench, and the Inner Zone on the north side (Fig. 2). Quaternary volcanism has occurred almost entirely north of the SW Japan arc except in southern Kyushu. Miocene near-trench magmatism occurred mainly in the Outer Zone and in the Setouchi province, part of the Inner Zone (Fig. 2). The basement of the Setouchi province consists of Jurassic accretionary complexes and Late Cretaceous granitic intrusions (Maruyama, 1997), and the basement of the Outer Zone consists of Triassic to Cretaceous metamorphic and accretionary complexes. The Shimanto Belt, a Cretaceous to early Miocene accretionary complex formed in cold hydrous fore-arc, is distributed south of the Butsuzo Tectonic Line (Taira, 1988), in the southernmost part of the Outer Zone. In Kyushu, the Usuki–Yatsushiro Tectonic Line is regarded as the extension of the Median Tectonic Line, though some researchers have disputed this interpretation based on the distribution of Mesozoic metamorphic complexes (Miyazaki *et al.* 2016).

Miocene near-trench magmatism is classified on the basis of lithology and distance from the Nankai Trench into three provinces, described below and summarized in Table 1.

2.a.1. Setouchi province

In the Setouchi province, the farthest from the trough, sporadically distributed volcanic rocks such as pitchstone, garnet-bearing dacite, and aphyric and glassy andesite compose the Setouchi Volcanic Rocks (Tatsumi, 2006). They are characterized by the production of high-Mg andesites, which are presumed to have been formed by the reaction of slab melt with peridotite in the mantle wedge based on their geochemical characteristics (Tatsumi, 2006). This assumption is reinforced by the presence of dacites and rhyolites with high Sr/Y ratios and depleted heavy rare-earth element with no or small Eu negative anomaly profiles consistent with slab melting (Shimoda & Tatsumi, 1999; Shinjoe *et al.* 2007).

2.a.2. Outer zone granitic rocks

The second province, south of the Median Tectonic Line, consists of voluminous felsic to intermediate igneous complexes here called the Outer Zone Granitic Rocks (OZGs). These complexes are mainly isolated plutons and volcano–plutonic complexes, some of which formed large calderas. OZGs closer to the trench have higher K_2O contents and alumina saturation indexes (molar $Al_2O_3/(CaO + Na_2O + K_2O)$) than those farther from the trench (Nakada & Takahashi, 1979; Shinjoe *et al.* 2007). A regional zonal gradation is recognized from S-type ilmenite-series granites near the trench to I-type ilmenite-series granites away from the trench (Ishihara, 1977; Takahashi *et al.* 1980; Murata & Yoshida, 1985). They are described here from east to west.

OZGs in the southern Kii Peninsula include the Ohmine Granitic Rocks (OGRs) and the Kumano Acidic Rocks (KARs) (Fig. 2). The OGRs consist, from north to south, of the Dorogawa, Shirakura, Kose, Asahi, Tenguyama and Shiratani plutons along with many satellite stocks and dikes of granitic to granodioritic composition. Murata (1982, 1984) classified the Dorogawa and Shirakura plutons as I-type granites and the others as S-type granites on the basis of their major-element compositions and petrography.

Along the eastern coast of the Kii Peninsula, the KARs extend over an area of ~600 km^2 and overlie early to middle Miocene sedimentary rocks of the Kumano Group. They are composed, in ascending order, of rhyolitic lava (Konogi rhyolite), ash-flow tuff (Owase–Shirahama pyroclastic rocks; Kawakami & Hoshi, 2007) and a laccolith of porphyritic granite (e.g. Aramaki & Hada, 1965; Miura & Wada, 2007). Based on their distribution, the KARs are divided into northern and southern units, and a large (41 × 23 km) trapdoor caldera structure, referred to here as the Kumano caldera, is recognized in the southern unit (Miura, 1999). An arcuate pyroclastic dike (Kozagawa dike) is exposed

https://doi.org/10.1017/S0016756819000785 Published online by Cambridge University Press

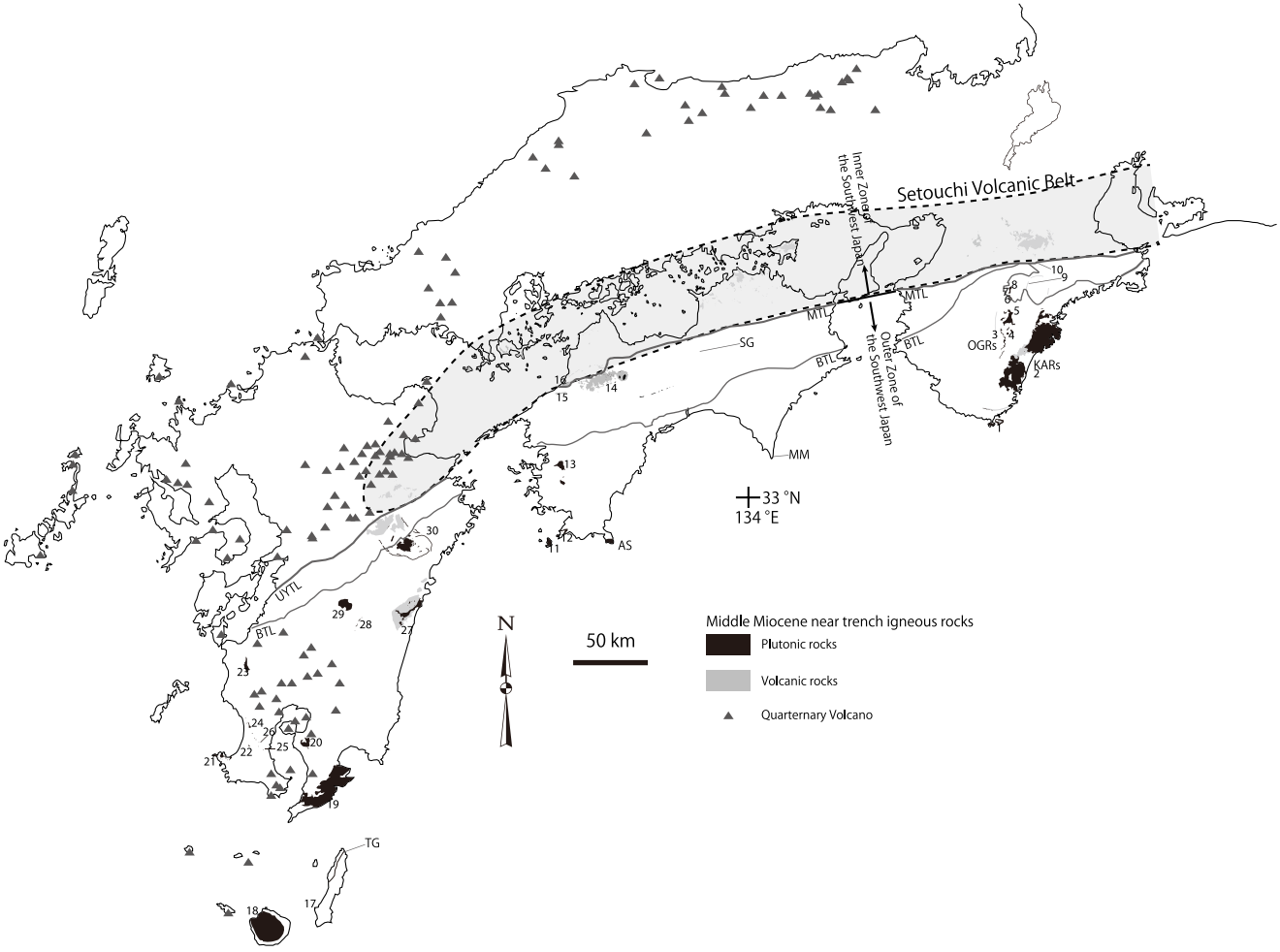

Fig. 2. Outline map of SW Japan showing the distribution of middle Miocene igneous rocks in the near-trench region of the SW Japan arc (compiled from Geological Survey of Japan, 2015). Abbreviations of tectonic features: MTL, Median Tectonic Line; BTL, Butsuzo Tectonic Line; UYTL, Usuki–Yatsushiro Tectonic Line. Abbreviations of igneous bodies: OGRs, Ohmine Granitic Rocks; KARs, Kumano Acidic Rocks; MM, Murotomisaki body; SG, Shingu alkali basalt dike; AS, Ashizuri igneous complex; TG, Tanegashima alkali dolerite dike. Numbers next to igneous bodies correspond to their entries in Table 1. Black triangles represent Quaternary volcanoes. Light grey shading indicates the Setouchi Volcanic Belt.

along its southern margin (Mizuno, 1957; Hoshi *et al.* 2013). A caldera collapse structure measuring 20 × 30 km is recognized in the northern unit (Kawakami *et al.* 2007).

The KARs have peraluminous compositions and commonly contain cordierite and garnet phenocrysts (Aramaki & Hada, 1965; Shinjoe *et al.* 2007), as in the S-type granites of the OGRs. A large batholith is inferred beneath the KARs and OGRs (Miura, 1999; Miura & Wada, 2007) from magnetotelluric evidence of a northward dipping high-resistivity rock mass beneath the Kumano caldera (Fujita *et al.* 1997), and extends beneath the OGRs where it connects with a deeper resistive body (Umeda *et al.* 2003). Another large caldera, the Ohmine–Odai caldera (Sato & YORG, 2006), is inferred from the presence of arcuate faults and pyroclastic dikes. It extends NW of the northern unit of the KARs where it overlaps exposures of the OGRs, the Nakaoku dike swarm (Wada & Iwano, 2001), and the Ohmine dike (Kimura, 1986). Related to the OGRs is the Takamiyama porphyritic granite, intruded along the Median Tectonic Line. Its S-type major-element composition and petrography (Wada & Araki, 1997) makes it an exception to the zonal arrangement of S-type and I-type granites.

In NW Shikoku, the Ishizuchi Group covers a 35 × 10 km area south of the Median Tectonic Line (Yoshida, 1984). In stratigraphically ascending order it consists of the Takano pyroclastic flow deposits, Kuromoritoge andesite, Saragamine andesite, Yoaketoge altered dacite and Tengudake pyroclastic flow deposits. These are intruded by ring dikes and the central Omogo pluton, an I-type granite. The upper three units are within the circular Ishizuchi caldera, which is defined by a system of arcuate faults *c.* 7 km in diameter (Yoshida, 1984; Takehara *et al.* 2017). In western Shikoku, the Myojinyama-type Acidic Rocks (Tazaki *et al.* 1993), felsic intrusions composed of holocrystalline dacite and rhyolite, are distributed along the Median Tectonic Line in lenticular exposures as long as 5 km. Southwesternmost Shikoku contains S-type granitic plutons and some satellite stocks (Fig. 2). The Okinoshima–Kashiwajima pluton, which intrudes Palaeogene rocks of the Shimanto accretionary complex, is subdivided into Tanijiri-type granodiorite and Mojima-type granite (Dai *et al.* 1993). The Uwajima pluton is composed of biotite granodiorite containing cordierite-bearing and hypersthene-bearing lithologies, although their order of intrusion is unclear (Shinjoe, 1997).

In Kyushu, the OZGs include caldera-forming volcano–plutonic complexes in the north and batholithic plutons in the south. In northern Kyushu, the caldera-forming Okueyama and Osuzuyama complexes, among other small plutons, are generally

https://doi.org/10.1017/S0016756819000785 Published online by Cambridge University Press

Table 1. Summary of geological background of the near-trench igneous bodies in SW Japan analysed in this study

No.	Igneous body name	Country rocks	Rock types	Previous dating results*
Kii Peninsula				
1	Shionomisaki	Kumano Formation(Early to Middle Miocene fore-arc basin sediment)	Tholeiitic basalt/gabbro, low K rhyolite lava, granophyre and felsite intrusions	13.1–15.2 Ma (FT zr)
2	Kumano	Kumano Formation(Early to Middle Miocene fore-arc basin sediment) and Shimanto belt (Late Cretaceous to Oligocene accretionary complex)	Rhyolitic lava, welded tuff, granite porphyry laccolith and ring dike (S-type) composing two calderas	13.8 Ma (K–Ar wr), 14.4-14.2 Ma (K–Ar bt), 11.8-18.0 Ma (FT zr)
3	Ohmine dike	Shimanto belt (Late Cretaceous accretionary complex)	Rhyolitic tuff dike composing the Ohmine caldera	n/a
4	Shiratani	Shimanto belt (Late Cretaceous accretionary complex)	Granite pluton (S-type)	14.7–15.6 Ma (K–Ar bt), 14.1–17.5 Ma (FT zr)
5	Tenguyama	Shimanto belt (Late Cretaceous accretionary complex)	Granite pluton (S-type)	15.1–17.3 (FT zr), 14.5–14.7 Ma(K–Ar bt)
6	Kose	Shimanto belt (Late Cretaceous accretionary complex) and Chichibu belt (Jurassic accretionary complex)	Granite pluton (S-type)	12.6–14.6 Ma (K–Ar bt), 14.2–15.2 Ma (FT zr)
7	Shirakura	Shimanto belt (Late Cretaceous accretionary complex) and Chichibu belt (Jurassic accretionary complex)	Granodiorite pluton (I-type)	14.2 Ma (K–Ar hbl), 14.6 Ma (K–Ar bt), 13.4 Ma (FT zr)
8	Dorogawa	Chichibu belt (Jurassic accretionary complex)	Granodiorite pluton (I-type)	11.6–12.1 Ma (K–Ar hbl, bt), 14.8–18.8 Ma (FT zr), 14.0 Ma (K–Ar bt)
9	Nakaoku dike	Chichibu belt (Jurassic accretionary complex)	Rhyolitic tuff dike composing the Odai caldera	14.7 Ma (FT zr)
10	Takamiyama	Sanbagawa metamorphic belt (Cretaceous high-pressure metamorphic rocks) and Ryoke granite (Late Cretaceous)	Quartz porphyry stock (S-type)	n/a
Western Shikoku				
11	Okinoshima	Shimanto belt (Eocene to Oligocene accretionary complex)	Granite/granodiorite pluton (S-type)	15 Ma (K–Ar bt) , 14.4–16 Ma (Rb–Sr wr)
12	Kashiwajima	Shimanto belt (Eocene to Oligocene accretionary complex)	Granite/granodiorite pluton (S-type)	16 Ma (Rb–Sr wr)
13	Uwajima	Shimanto belt (Late Cretaceous accretionary complex)	Granodiorite pluton (S-type)	12–14.0 Ma (K–Ar bt) 15.0 Ma (FT zr)
14	Ishizuchi	Sanbagawa metamorphic belt (Cretaceous high-pressure metamorphic rocks) and Kuma Formation (Early to Middle Miocene non-marine sediment)	Dacitic/rhyolitic welded tuff, andesite lava, decitic welded tuff and granodiorite pluton (Ishizuchi cauldron; I-type)	14 Ma (K–Ar bt), 12.8–15.4 (K–Ar wr, pl), 14.21–14.80 Ma (U–Pb zr)
15	Ishidatami	Sanbagawa metamorphic belt (Cretaceous high-pressure metamorphic rocks)	Dacite intrusion	14.1 Ma (K–Ar wr)
16	Myojin-yama	Izumi Formation (Late Cretaceous fore-arc basin sediment)	Rhyolite intrusion	13.9–14.3 Ma (K–Ar wr)
Kyushu				
17	Tanegashima	Kumage Formation (Palaeogene accretionary complex)	Quartz porphyry stock (S-type)	15.6 Ma (K–Ar wr)
18	Yakushima	Kumage Formation (Palaeogene accretionary complex)	Granite pluton (S-type)	12.9–15.7 Ma (K–Ar wr), 12.2–15.6 Ma (K–Ar bt), 14.2–15.3 Ma (K–Ar ksp)
19	Minami-Osumi	Shimanto belt (Eocene to Oligocene accretionary complex)	Granite pluton (S-type)	13.4–14.4 Ma (K–Ar–bt), 13.1–14.0 Ma (FT zr)
20	Takakumayama	Shimanto belt (Late Cretaceous accretionary complex)	Granite pluton (S-type)	16 Ma (K–Ar bt), 12.9 Ma (FT zr)
21	Nomamisaki	Shimanto belt (Early to Late Cretaceous accretionary complex)	Granodiorite stock (I-type)	12 Ma (K–Ar wr)

(*Continued*)

https://doi.org/10.1017/S0016756819000785 Published online by Cambridge University Press

Table 1. (*Continued*)

No.	Igneous body name	Country rocks	Rock types	Previous dating results*
22	Kimposan	Shimanto belt (Early to Late Cretaceous accretionary complex)	Granodiorite stock (I-type)	13.6 Ma (K–Ar wr), 14.6 Ma (FT zr)
23	Shibisan	Shimanto belt (Early to Late Cretaceous accretionary complex)	Granodiorite pluton (I-type)	15 Ma (K–Ar bt), 12.3–12.7 Ma (FT zr)
24	Hioki	Shimanto belt (Early to Late Cretaceous accretionary complex)	Granodiorite stock (I-type)	12.2 Ma (K–Ar bt)23, 14.4 Ma (FT zr)26
25	Akanita	Shimanto belt (Late Cretaceous accretionary complex)	Granodiorite stock (I-type)	20.1 Ma (K–Ar wr), 13.9 Ma (FT zr)
26	NE Kumagatake	Shimanto belt (Late Cretaceous accretionary complex)	Granodiorite stock (I-type)	n/a
27	Osuzuyama	Shimanto belt (Eocene to Oligocene accretionary complex)	Granodiorite porphyry, welded tuff, volcanic breccia (S-type) composing a caldera	13–15.6 Ma (K–Ar bt, wr) 14.9 Ma (FT zr)
28	Murasho	Shimanto belt (Eocene to Oligocene accretionary complex)	Granite porphyry dike (S-type)	14.3 Ma (FT zr)
29	Ichifusayama	Shimanto belt (Late Cretaceous to Oligocene accretionary complex)	Granodiorite pluton (I-type)	13.31–14 Ma (K–Ar bt) 12.3–13.3 Ma (FT zr)
30	Okueyama	Shimanto belt (Late Cretaceous to Oligocene accretionary complex) and Chichibu belt (Jurassic accretionary complex)	Dacitic/rhyolitic welded tuff, rhyolite lava, andesite lava, granodiorite batholith (I-type), granite porphry ring dike composing three calderas	13.8 Ma (K–Ar bt), 13.7 Ma (Rb–Sr wr), 12.4–12.8 Ma(K–Ar wr)

*Reference and individual data are listed in the Supplementary Material (S10) (https://doi.org/10.1017/S0016756819000785). Abbreviations for the analysed samples are as follows: zr, zircon; wr, whole rock; bt, biotite; pl, plagioclase; ksp, K-feldspar; hbl, hornblende.

S-type granites on the trench side (Yakushima, Minami–Osumi, Takakumayama, Murasho and Osuzuyama) and I-type granites on the back-arc side (Nakada & Takahashi, 1979). The Okueyama complex is a deeply eroded Valles-type caldera nested within a vertically zoned granitic batholith, and their combined original volume is estimated to exceed 1000 km^3 (Takahashi, 1986*a*; Takahashi *et al.* 2014). Three phases of activity are recognized: formation of the Sobosan cauldron (18 × 13 km) and Katamukiyama cauldron (12 × 6 km), development of andesite/dacite composite volcanoes within the calderas, and formation of the Okueyama cauldron (33 × 23 km), which was preceded by the eruption of the Kunimidake rhyolitic tuff and followed by intrusion of the Okueyama batholith (Takahashi, 1986*a*). The Okueyama cauldron is surrounded by ring dikes of porphyritic granite. The Osuzuyama volcano–plutonic complex is composed of a porphyritic granitic intrusion accompanied by small granite stocks and overlying volcanic breccia and welded tuff, all of which are presumed to be comagmatic and derived from a single magma chamber (Nakada, 1983). In southern Kyushu, the batholithic Yakushima pluton (25 × 20 km) and Minami–Osumi pluton (48 × 15 km) intrude Palaeogene rocks of the Shimanto accretionary complex.

2.a.3. Marginal zone igneous rocks

The third province, Marginal Zone Igneous Rocks (after Takahashi, 1986*b*), is closest to the Nankai trough and consists of intrusive alkaline and tholeiitic basaltic rocks, with or without accompanying felsic intrusive rocks. Alkaline basaltic rocks are present at three localities (Fig. 2): the Tanegashima alkali dolerite dike on Tanegashima Island south of Kyushu (Taneda & Kinoshita, 1972), the Ashizuri igneous complex in southernmost Shikoku (Murakami *et al.* 1989), and the Shingu alkali basalt dikes in north-central Shikoku (Uto *et al.* 1987). The Ashizuri complex is accompanied by felsic lithologies such as syenite and alkali granite. A tholeiitic gabbro sill 2 km long and up to 230 m thick intrudes the Eocene to early Miocene accretionary complex of the Shimanto Belt at Cape Murotomisaki in SE Shikoku (Akatsuka *et al.* 1999) (Fig. 2), and a tholeiitic gabbro/basalt intrusion accompanies felsic effusive and intrusive rocks at Cape Shionomisaki at the southern tip of the Kii Peninsula (Miyake, 1985). These tholeiitic basalts have mid-ocean ridge basalt (MORB)-like geochemical characteristics and are thought to be the product of a subducted spreading ridge during the waning stage of the opening of the Shikoku Basin (Takahashi, 1986*b*; Yamaji & Yoshida, 1998; Kimura *et al.* 2005).

2.a.4. Samples

We collected samples from Miocene felsic rocks of the Outer Zone, from the Kii Peninsula to Kyushu, for zircon U–Pb age determinations. Most samples were from OZGs. Samples were collected from the Ashizuri igneous complex and Shionomisaki Igneous Complex of the Marginal Zone Igneous Rocks, and zircon U–Pb ages for the Ashizuri igneous complex have previously been reported by Shinjoe *et al.* (2010). Two zircon-bearing mafic rocks from the Shionomisaki Igneous Complex were also sampled for U–Pb age determinations.

2.b. Geochemistry of felsic rocks of the Outer Zone

This section briefly describes the whole-rock geochemistry of the felsic rocks of the Outer Zone. The SiO_2 contents of the felsic rocks range from 65 to 80 wt %, and major oxides are plotted against SiO_2 in Figure 3. In these variation diagrams, samples from the Kii Peninsula, western Shikoku and Kyushu plot in almost the same areas, forming broad trends with SiO_2 content. Some of

https://doi.org/10.1017/S0016756819000785 Published online by Cambridge University Press

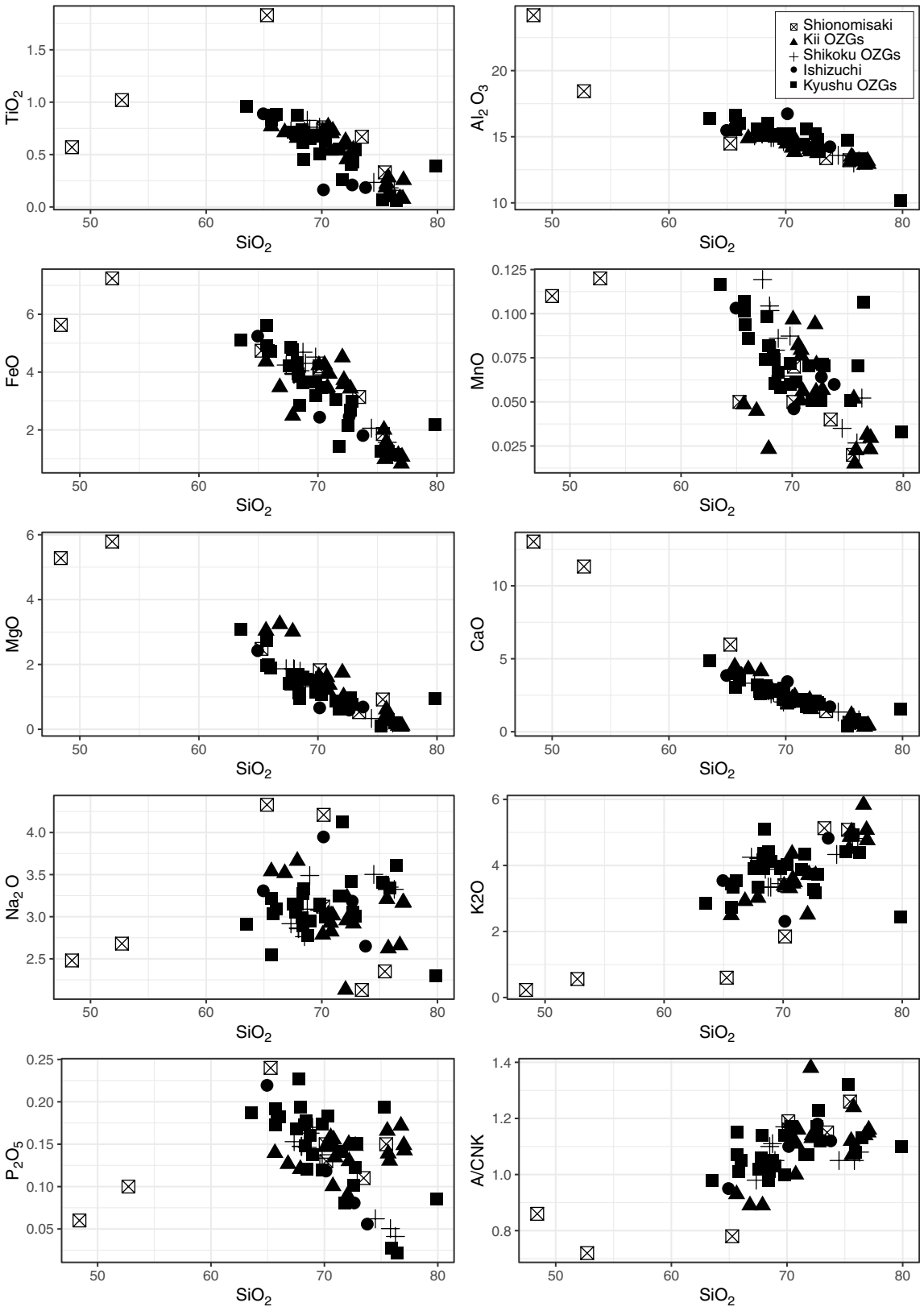

Fig. 3. Major-element variation diagrams for the felsic rocks of the Outer Zone. Samples from the Shionomisaki igneous complex include two mafic rocks and a rhyolite. Most of the data points are for the samples used for the zircon U–Pb analysis, but some are for different samples of similar lithology. Data are from Ogasawara (1997), Anma *et al*. (1998), Shinjoe *et al*. (2007) and Shinjoe (unpublished data). A/CNK, Alumina saturation index.

https://doi.org/10.1017/S0016756819000785 Published online by Cambridge University Press

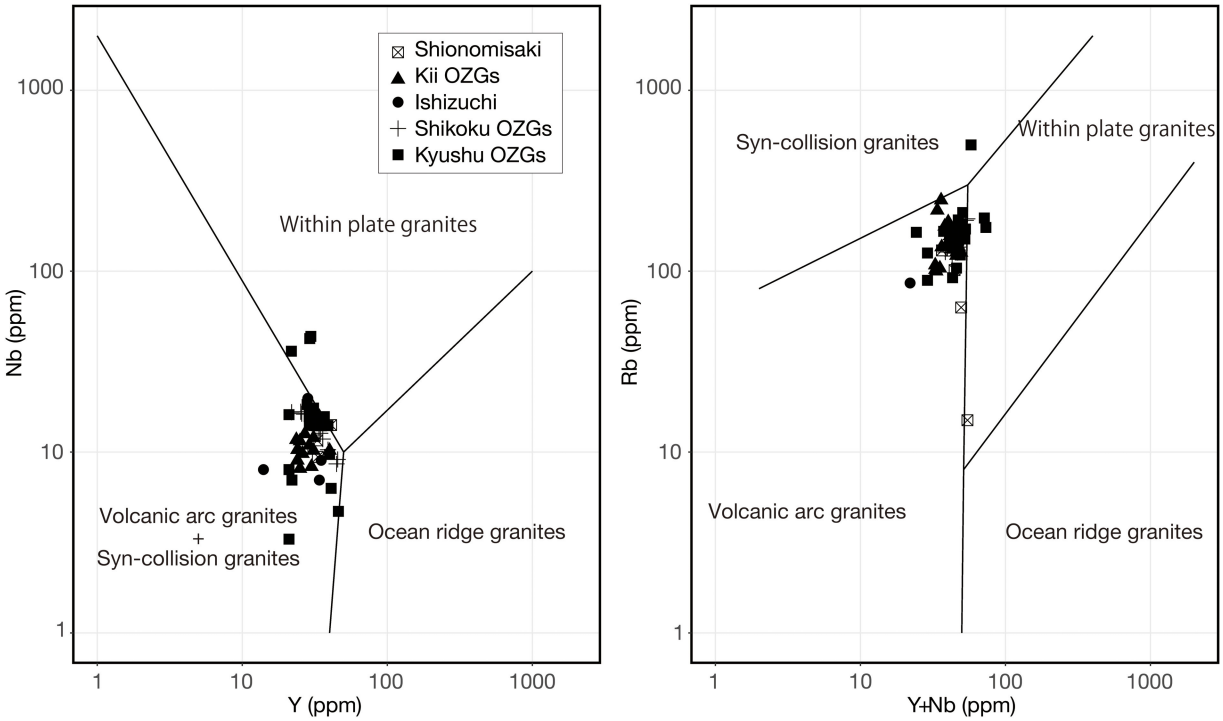

Fig. 4. Y–Nb and (Y + Nb) – Rb discrimination diagrams (Pearce *et al.* 1984) showing the classification of felsic rocks of the Outer Zone of the SW Japan arc.

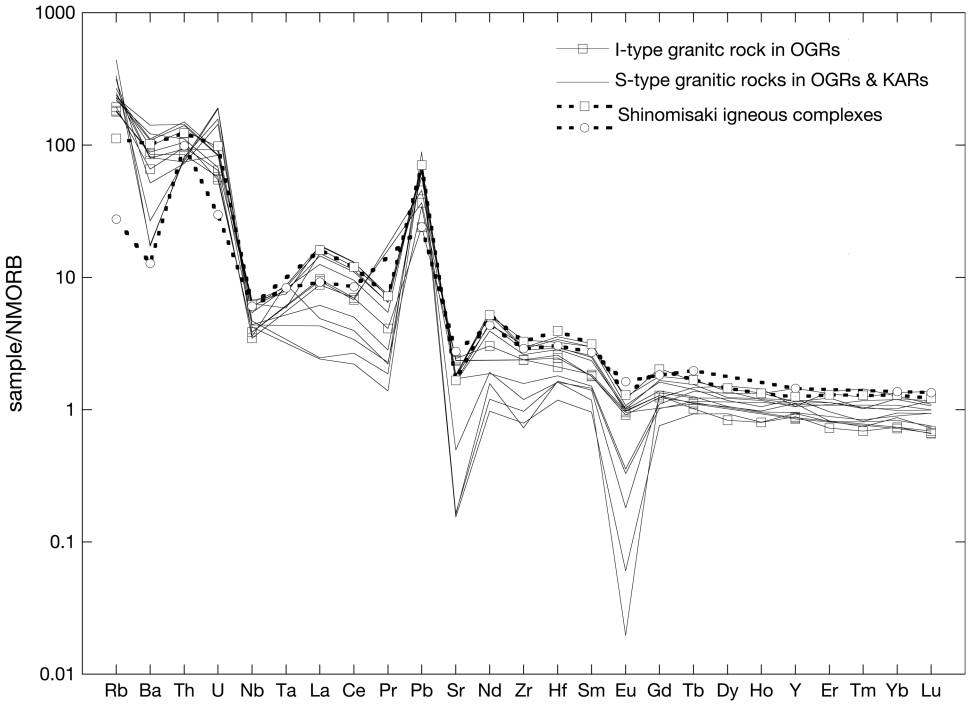

Fig. 5. Whole-rock trace-element compositions of selected felsic rocks in the Kii Peninsula (data from Shinjoe *et al.* 2007), normalized to normal MORB (Sun & McDonough, 1989).

the felsic rocks of the Shionomisaki Igneous Complex have low K_2O contents that clearly differ from those of the S-type OZGs in the same region (Shinjoe *et al.* 2007). Most of the samples have alumina saturation index values greater than 1.0, except for those with relatively low SiO_2 content (Fig. 3).

Trace-element evidence that distinguishes four broad tectonic categories (Pearce *et al.* 1984) shows that nearly all of our samples fall in the field of volcanic arc granites (Fig. 4). The incompatible element profiles of Outer Zone felsic rocks in the Kii Peninsula (Shinjoe *et al.* 2007), shown in Figure 5, indicate that the I-type and S-type granites of the OZGs are enriched in large-ion lithophile elements and slightly depleted in Nb and Ta, whereas Ba, Sr and Eu are depleted to various degrees depending on the extent of feldspar fractionation. In the K-poor felsic rocks of the Shionomisaki Igneous Complex, large-ion lithophile elements are only weakly enriched.

https://doi.org/10.1017/S0016756819000785 Published online by Cambridge University Press

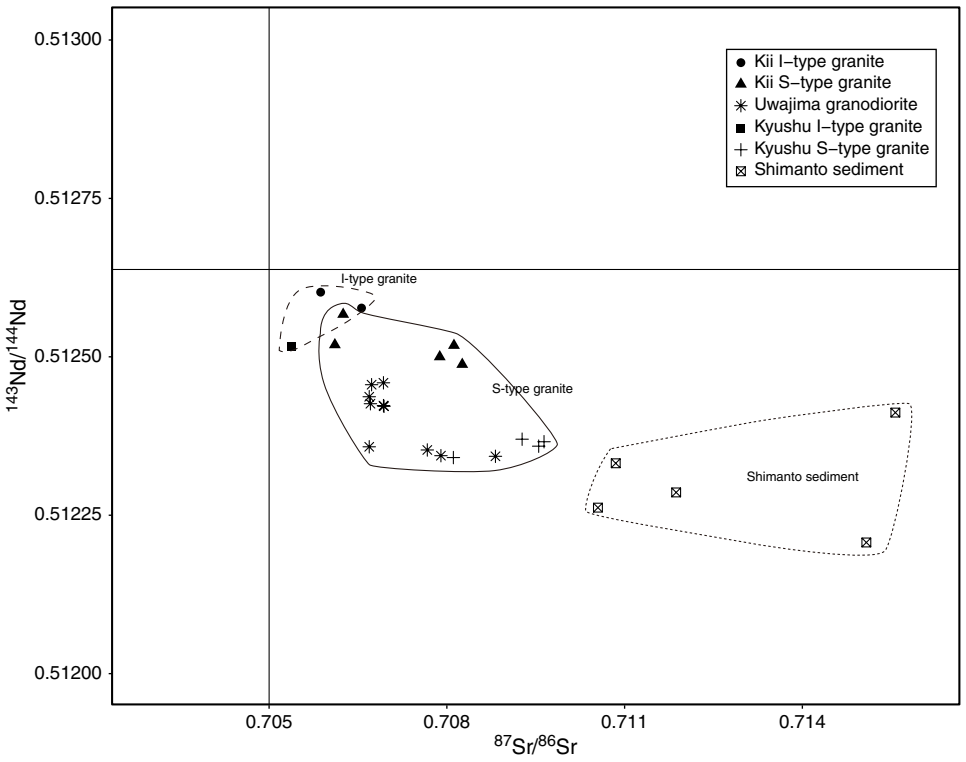

Fig. 6. Sr and Nd isotopic compositions of felsic plutonic rocks in the Outer Zone of the SW Japan arc (data from Terakado *et al.* 1988; Shinjoe, 1997).

OZGs from the Kii Peninsula and Kyushu (Terakado *et al.* 1988) and the Uwajima pluton of SW Shikoku (Shinjoe, 1997) have $^{87}Sr/^{86}Sr$ ratios of 0.7054–0.7066 for I-type granites and 0.7061–0.7093 for S-type granites, and $^{143}Nd/^{144}Nd$ ratios of 0.51252–0.51260 for I-type granites and 0.51230–0.51257 for S-type granites. These Sr and Nd isotopic compositions are enriched compared to the present bulk Earth; however, these granites have lower $^{87}Sr/^{86}Sr$ and higher $^{143}Nd/^{144}Nd$ ratios than the sedimentary rocks of the Shimanto accretionary complex (Fig. 6). It appears that the magma source for these OZGs, even the S-type granites, included a mantle-derived component (Shinjoe, 1997).

2.c. Previous geochronological constraints

Previous radiometric dates for the OZGs were mainly determined using K–Ar methods (Shibata & Nozawa, 1967). Shibata (1978) re-examined some samples with controversial ages and concluded that the OZGs formed at 14 ± 1 Ma. Later researchers have used K–Ar and fission-track methods and obtained generally consistent results (e.g. Sumii *et al.* 1998; Sumii, 2000; Iwano *et al.* 2007). Previous radiometric ages for the OZGs are presented in Figure 7 and summarized for each igneous body in Table 1. Although most of the ages are concentrated between 13 and 16 Ma, outliers extend from 12 to 22 Ma. This scatter may be the result of excess Ar or Ar loss that affects samples in K–Ar dating. It is noteworthy that all K–Ar ages represent cooling ages. Hence it is crucial to constrain the age of magmatism by zircon U–Pb dating, taking advantage of the higher closure temperatures in zircon, to shed light on the relationship between fore-arc magmatism and clockwise rotation of the SW Japan arc during and after Miocene time.

3. Methodology

U–Pb ages of zircon were determined using a VG Plasma Quad 3 inductively coupled plasma mass spectrometer (ICP-MS) at the Earthquake Research Institute of the University of Tokyo, connected to a frequency quintupled ($\lambda = 213$ nm) Nd-YAG laser ablation (LA) system (New Wave Research UP-213). Details of the analytical protocol, precision and accuracy of the zircon U–Pb dating are presented in Orihashi *et al.* (2008), and the analytical conditions are listed in Table 2. The ISOPLOT 4.15 program (Ludwig, 2012) was used for calculation of weighted means, mean square weighted deviations (MSWDs) and probabilities and for plotting data on a Tera–Wasserberg concordia diagram. Replicate measurements of the 91500 zircon standard ($n = 333$) during this study yielded a ^{238}U–^{206}Pb age of 1051.9 ± 3.3 Ma (weighted mean age ±95 % confidence) and a ^{235}U–^{207}Pb age of 1063.5 ± 2.5 Ma (weighted mean age ±95 % confidence). Deviations from the isotope dilution thermal ionization mass spectrometry (ID-TIMS) data (1062.4 ± 0.4 Ma and 1063.5 ± 0.3 Ma, respectively) reported by Wiedenbeck *et al.* (1995) are within 1 %. Replicate measurements of the OD-3 zircon standard ($n = 115$) yielded a ^{238}U–^{206}Pb age of 32.73 ± 0.22 Ma (weighted mean age ±95 % confidence) and a ^{235}U–^{207}Pb age of 33.44 ± 0.38 Ma (weighted mean age ±95 % confidence), which are consistent with the weighted mean ^{238}U–^{206}Pb age (33.0 ± 0.1 Ma) of multiple-laboratory comparison data (Iwano *et al.* 2013) and the ID-TIMS value of 32.72 ± 0.16 Ma reported by Lukács *et al.* (2015).

4. Results

Our U–Pb analyses emphasized the rims of euhedral zircon grains to determine the magmatic age of the samples. To avoid inclusions

https://doi.org/10.1017/S0016756819000785 Published online by Cambridge University Press

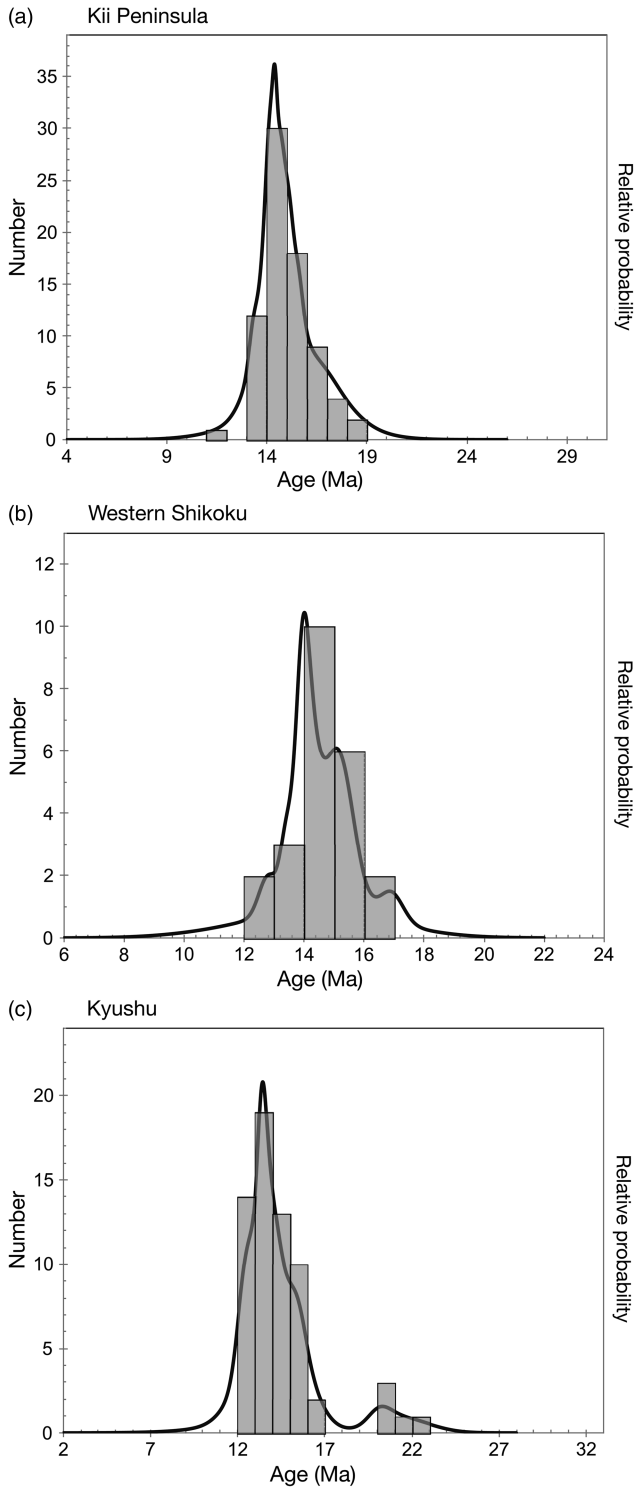

Fig. 7. Probability density plots and histograms of previously reported radiometric ages of the OZGs in the SW Japan arc: (a) Kii Peninsula (from Iwano *et al.* 2007), (b) Western Shikoku (from Shinjoe & Sumii, 2001) and (c) Kyushu (from Shinjoe & Sumii, 2003; Oikawa *et al.* 2006). Ages were determined by K–Ar or zircon fission-track methods, plus a few obtained by the Rb–Sr whole-rock isochron method.

and fractures at the analytical points, zircon grains were monitored under a transmitted light microscope during laser ablation. Samples were observed by cathodoluminescence (CL) and back-scattered electron images before or after analysis except for some early samples. CL images showing representative zonal structures including both I-type and S-type granitic rocks are presented in Figure 8.

For each rock sample, 23–81 points were measured and weighted means, shown in Table 3, were obtained from five or more concordant ^{238}U–^{206}Pb ages of primary magmatic zircons. Most of the samples comprise many discordant analytical points explained in terms of Pb loss for older inherited grains or contamination of common Pb. In this research, correction of common Pb was not conducted. Hg contamination in the Ar carrier gas is unavoidable in the LA-ICP-MS method, hence highly accurate ^{204}Pb determination is very difficult due to the interference of ^{204}Hg. Common Pb correction using $^{208}Pb/^{232}Th$ ratio (Anderson, 2002) is also not appropriate in our approach. The analytical method by Orihashi *et al.* (2008) is used in this study, optimized so that the ablation fractionation is minimized at the $^{206}Pb/^{238}U$ ratio. Under this analytical condition, error at the $^{208}Pb/^{232}Th$ ratio in repeated analysis of the standard reached up to *c.* 15 % (2σ), resulting in analytical errors much larger than those of $^{206}Pb/^{238}U$ age.

Rather than attempting to apply a common-Pb correction, we have used a regression technique, treating our population of analyses as representing mixtures between the common-Pb and radiogenic-Pb components. First, we select only the concordant analysis, then calculate the weighted mean of the $^{206}Pb/^{238}U$ age for concordant analytical points. Concordant but older inherited zircons in each sample were statistically distinguished from the weighted mean data of primary magmatic zircons. After excluding analytical points of inherited grains, the lower intercept age is determined by regression. If this agrees with the weighted mean of the concordant age of primary magmatic zircons within the error range, and the $^{207}Pb/^{206}Pb$ ratio of the other end component is close to that of common Pb (Stacey & Kramers, 1975), the selected population of discordant points were considered to be affected by common Pb for primary magmatic zircons. The agreement between the lower intercept age and the weighted mean age strengthens the legitimacy of the concordant analytical point judged as 'primary magmatic zircon'. Lower intercept ages are also listed in Table 3, except for two samples for which an effective regression line could not be obtained due to the poor population affected by common Pb. Tera–Wasserburg diagrams including regression line and plots showing the result of weighted mean calculation for representative samples are shown in Figure 9. Analytical data are listed in Supplementalry Material Tables S3–S11 (https://doi.org/10.1017/S0016756819000785). Plots of the Tera–Wasserburg diagram and weighted mean calculation results for all samples are included in the Supplementary Material S12 (https://doi.org/10.1017/S0016756819000785).

Relative density plots and histograms of ^{238}U–^{206}Pb ages for each region are shown in Figure 10. ^{238}U–^{206}Pb ages of samples from the Kii Peninsula (13.59–15.60 Ma), Shikoku (14.14–15.23 Ma) and Kyushu (13.46–15.56 Ma) are in good agreement. The narrower age range of samples from Shikoku probably reflects the smaller number of data. The distribution of Miocene igneous rocks and the overall results of U–Pb analysis of each region are shown in Figures 11–13.

4.a. Kii Peninsula

4.a.1. Shionomisaki igneous complex

The Shionomisaki Igneous Complex, at the southern tip of the Kii Peninsula, is composed of mafic to felsic intrusive and extrusive rocks (Fig. 14). Our zircon U–Pb analysis for three samples

https://doi.org/10.1017/S0016756819000785 Published online by Cambridge University Press

Table 2. Summary of LA–ICP–MS operating conditions

ICP-MS		Laser ablation	
Model	Thermo Elemental Plasma Quad3	Model	New Wave Research UP213
Forward power	1380 W	Laser type	UV 213 nm (frequency quadrupled Nd-YAG laser)
Lens	VG CHICANE Lens	Energy density	11–13 J cm^{-2}
Ar gas flow rate	Cool 13.5 L min^{-1}	Crater size	30 mm
	Auxiliary 1.0 L min^{-1}	Repetition rate	10 Hz
	Nebuliser 0.9–1.1 L min^{-1}	Pre-ablation	3 s
He gas flow rate	0.7–0.8 L min^{-1}	Carrier gas	He
N_2 gas flow rate	0.8 mL min^{-1}	Focus	Fixed focus on sample surface
Expansion pump	S-option		
Scanning mode	Peak jump		
Integration time	20 s		
Monitor isotope	^{202}Hg, ^{204}Pb, ^{206}Pb, ^{207}Pb, ^{208}Pb, ^{232}Th, ^{238}U		
Standard	NIST SRM610		

(SP202, SP205 and SP212 in Table 3) yielded ^{238}U–^{206}Pb weighted mean ages of a dolerite, a gabbroic intrusion and a rhyolite lava ranging from 14.61 to 15.38 Ma. Our results refined zircon fission-track ages reported by Hoshi *et al.* (2003) that ranged from 13.9 to 15.2 Ma with the exception of a 13.1 Ma felsite dike (Fig. 7).

4.a.2. OZGs in the Kii Peninsula

^{238}U–^{206}Pb ages were obtained for six samples from the KARs yielded weighted mean ages ranging from 14.48 to 15.51 Ma (Fig. 15). Welded tuff from the Owase-Shirahama pyroclastic rocks (sample IuchiWT) recovered from a borehole that penetrated a laccolith of porphyritic granite of the northern unit into the welded tuff (Kitagawa *et al.* 2009). Granite porphyry sample KUM16, collected from an isolated small peninsula of the southern unit, yielded a weighted mean age that did not overlap with other data within the error range, suggesting that precursory activity occurred there before the majority of the KARs were emplaced.

We obtained ^{238}U–^{206}Pb ages of 14.88 ± 0.45 Ma and 14.67 ± 0.26 Ma for tuffite from the Ohmine dike (sample TKG1) and the Nakaoku dike (sample D1), respectively. These are within the age range of the KARs.

^{238}U–^{206}Pb ages of four S-type plutons of the OGRs ranged from 14.99 to 15.60 Ma. The Dorogawa pluton, the northernmost I-type pluton, yielded a ^{238}U–^{206}Pb age of 14.13 ± 0.29 Ma, youngest among the OGRs. Granodiorite of this pluton is characterized by low FeO*/MgO ratios, high Cr and Ni contents, and enclaves of high-Mg andesite-like diorite containing Cr-rich spinel, which suggests that it was derived from a high-Mg andesite magma, as reported for Setouchi Volcanic Rocks (Shinjoe *et al.* 2005). The Takamiyama pluton yielded a ^{238}U–^{206}Pb age of 13.59 ± 0.22 Ma, ~1 Ma younger than the major igneous activity of the OGRs.

Overall, the ^{238}U–^{206}Pb ages from the KARs and OGRs of the Shionomisaki Igneous Complex are in good agreement except for the two northernmost plutons (Dorogawa and Takamiyama plutons).

4.b. Western Shikoku

We obtained six ^{238}U–^{206}Pb ages from two S-type plutons (Okinoshima–Kashiwajima and Uwajima plutons) in western Shikoku (Fig. 11). In the Okinoshima–Kashiwajima pluton, Tanijiri-type granodorite is intruded by Mojima-type granite (Dai *et al.* 1993). For Tanijiri-type granodorite (samples OK2C and KAS2) we obtained ages of 14.71 ± 0.45 Ma and 14.99 ± 0.32 Ma, and for Mojima-type granite (sample OK1B) we obtained an age of 14.14 ± 0.18 Ma. Although our results are consistent with the order of intrusion, these ages accord with each other within their 2σ errors. From the Uwajima pluton we obtained ^{238}U–^{206}Pb ages for three samples with different mineral assemblages. The weighted mean ages range from 14.93 to 15.23 Ma and coincide with each other within their 2σ errors.

For the felsic rocks of the Ishizuchi Group, we obtained ^{238}U–^{206}Pb ages of 14.48 ± 0.16 Ma from a rhyolitic welded tuff (sample EHI100) of the lowest horizon Takano pyroclastic flow deposits and 14.35 ± 0.16 Ma from a granodiorite (sample EHI38) of the Omogo central pluton (Fig. 12). For the Myojinyama-type Acidic Rocks, we determined ^{238}U–^{206}Pb ages of 14.37 ± 0.16 Ma and 14.49 ± 0.15 Ma from dacites of the Ishidatami body (sample EHI105) and Myojinyama body (sample EHI205), respectively. These ages coincide with those of the adjacent Ishizuchi Group and previous whole-rock K–Ar ages reported by Tazaki *et al.* (1993) within their 2σ errors.

4.c. Kyushu

All of the analysed samples from Kyushu were collected from OZGs. We selected 21 samples from representative lithologies of 14 igneous bodies (Table 3; Fig. 13). Two older ages (15.48 ± 0.22 Ma and 15.56 ± 0.28 Ma) were obtained from quartz porphyry dikes on Tanegashima and Yakushima islands (Fig. 2), the nearest to the trench. These ages are comparable to the older KARs and OGRs in the Kii Peninsula. The other ages are concentrated within a range of 1.5 Ma (13.46 to 14.93 Ma).

https://doi.org/10.1017/S0016756819000785 Published online by Cambridge University Press

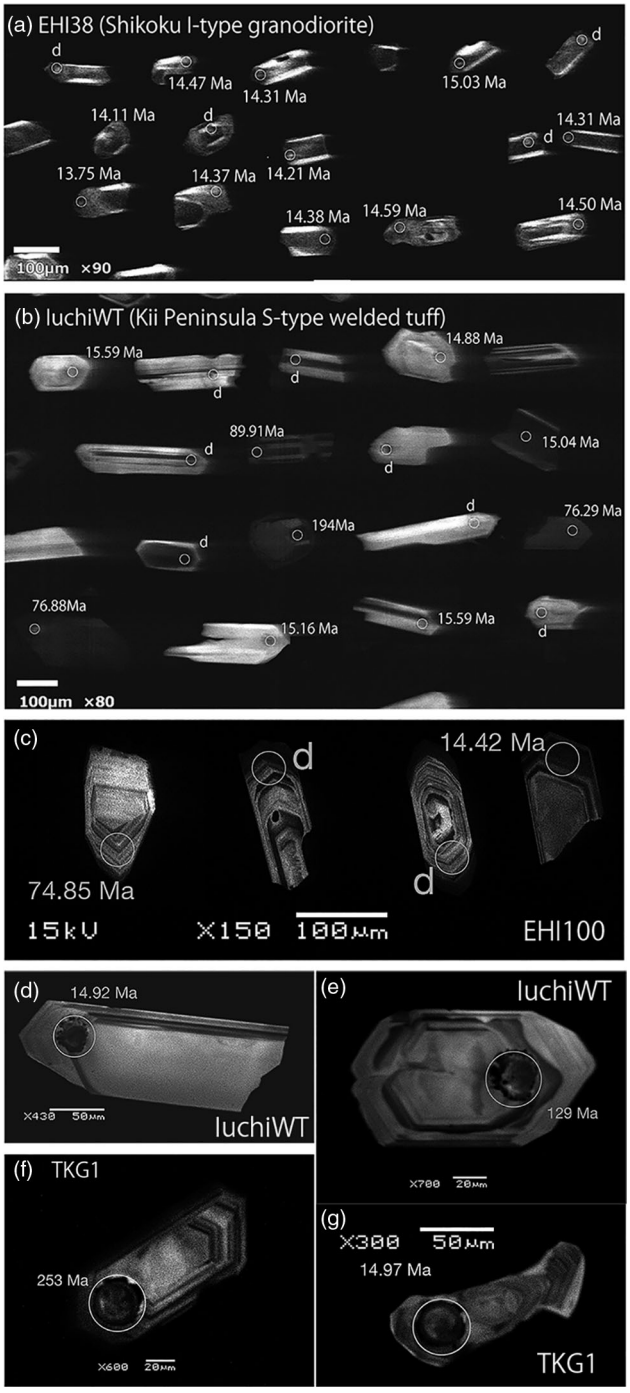

Fig. 8. Cathodoluminescence images showing representative zonal structures of analysed zircon grains. (a) I-type granodiorite in western Shikoku (EHI38), (b) welded tuff of the S-type Kumano Acidic Rocks in Kii Peninsula. We conducted LA-ICP-MS analysis mainly on the rim of the zircon crystals to constrain the magmatic age of the samples. Generally, most of the rim of the euhedral zircons of I-type granitic rocks yielded concordant primary magmatic ages, though some grains have dark core in CL images (a). Discordant analytical points (marked 'd') were presumed to be affected by common Pb (see Fig. 9). S-type granitic rocks usually contain a considerable amount of inherited zircons. For example, some of the rims for euhedral grains in S-type rhyolitic welded tuff (b) show Mesozoic ages. (c) Euhedral grains with concentric oscillatory zoning (from sample EHI100). These usually yielded concordant magmatic ages (right-hand grain), although some showed discordant results affected by common lead (analytical points marked 'd') or concordant older ages (left-hand grain). (d) Euhedral grains with oscillatory zoning rims and homogeneous cores (from sample IuchiWT) yielded concordant magmatic ages. (e) Euhedral grains with thin (<20 μm) rims with oscillatory zoning and intricately zoned cores showing concordant Cretaceous ages (from sample IuchiWT). (f) Euhedral grains showing concentric oscillatory zoning (from sample TKG1) with concordant Permian ages. (g) Anhedral grains with rims with oscillatory zoning yielded concordant magmatic ages (from sample TKG1).

For the batholithic Yakushima pluton, we analysed three zircon samples from the main-facies granite (sample YMG), orthoclase megacrysts (sample YKF) in the same granite, and a cordierite-bearing granodiorite (sample YYG). Although the Sr–Nd isotopic ratio of sample YYG implied strong sediment contamination (Anma *et al.* 1998; Kawano *et al.* 2007) and the inclusion mineralogy suggested that the orthoclase megacrysts crystallized relatively early (Kawachi & Sato, 1978; Anma, 1997), the three results from this pluton coincided with each other within their error ranges (Fig. 16). Two S-type plutons in the Osumi Peninsula of southernmost Kyushu (Minami–Oshumi and Takakumayama) yielded ages of 14.74 ± 0.17 Ma and 14.14 ± 0.31 Ma. Granite samples from the Ichifusayama pluton contained no primary magmatic zircon, only inherited zircons with ages ranging from Jurassic to Proterozoic.

Samples from four small plutons in southwesternmost Kyushu (samples SA101A, SA102, SA106 and SA107) yielded ^{238}U–^{206}Pb ages ranging from 14.25 to 14.93 Ma, which refine the previously reported older cluster ages of ~20 to 22 Ma (Fig. 2) obtained using the zircon fission-track method (MITI, 1985).

From the Okueyama volcano–plutonic complex, we obtained ^{238}U–^{206}Pb ages of 14.09 ± 0.19 Ma for the Sobosan andesite (sample MYA02), 14.00 ± 0.24 Ma for the Kunimidake rhyolitic tuff (sample MYA01), 13.70 ± 0.13 Ma for a granite of the Okueyama batholith (sample MYA03), and 14.28 ± 0.26 Ma for a porphyritic granite of the ring dike (sample MYA05).

From the Osuzuyama volcano–plutonic complex, porphyritic granodiorite stock yielded ^{238}U–^{206}Pb ages of 14.70 ± 0.37 Ma. The youngest ages among the OZGs in Kyushu were obtained for the Shibisan pluton (13.50 ± 0.15 Ma and 13.46 ± 0.30 Ma), the farthest from the trench axis.

5. Discussion

Our U–Pb dates for igneous rocks in the Outer Zone indicate that magmatism was active at the same time along the SW Japan arc from the Kii Peninsula to Kyushu, commencing at *c.* 15.6 Ma. This finding has implications for the opening of the Japan Sea, migration of the Philippine Sea plate and subduction of young and hot lithosphere of the Shikoku Basin during Miocene time, and the duration of caldera-forming eruptions in the Outer Zone.

5.a. Chronological relationship with the opening of the Japan Sea

Palaeomagnetic studies have established that both the SW and NE Japan arcs underwent rapid rotation in early to middle Miocene time. Early studies proposed that the SW Japan arc rotated clockwise ~50°, most of the rotation occurring between 16.1 and 14.2 Ma (Otofuji & Matsuda, 1983, 1987; Hayashida & Itoh, 1984; Otofuji *et al.* 1991). Subsequent research has pushed the dates of this rotation back in time. Nakajima *et al.* (1990) used K–Ar ages and palaeomagnetic evidence from Miocene rocks in Fukui, in the NE part of the arc, to show that the rapid rotation began at ~17 Ma and ceased at 15 Ma. Similar evidence for the rotation ending ~15 Ma was later reported from other sites in the arc (Hoshi *et al.* 2000; Hoshi & Sano, 2013). More recently, Sawada *et al.* (2013) re-examined the volcanic rocks in the Matsue area on the north side of the arc, originally investigated by Otofuji & Matsuda (1983) and Otofuji *et al.* (1991), and concluded that the clockwise rotation began after 18 Ma and ceased at 16 Ma, although their conclusion still depended on conventional

https://doi.org/10.1017/S0016756819000785 Published online by Cambridge University Press

Table 3. Results of zircon U–Pb ages

No.	Igneous body name	Sample code	Latitude	Longitude	Rock type	Occurrence	No. total data	Weighted mean of ^{238}U–^{206}Pb ages					Lower intercept age			
								*N**	age (Ma)		Error (95 % conf.)	MSWD	age (Ma)		Error (95 % conf.)	MSWD
Kii Peninsula																
1	Shionomisaki	SP202	33.4429°	135.7561°	Dolerite	Stock	30	14	**14.60**	±	**0.22**	**1.7**	14.69	±	0.29	5.4
		SP205	33.4645°	135.7985°	Rhyolite	Lava	35	19	**15.01**	±	**0.19**	**2.7**	14.92	±	0.23	2.7
		SP212	33.4460°	135.7689°	Gabbro	Stock	28	10	**15.38**	±	**0.29**	**1.9**	15.21	±	0.28	5.2
2	Kumano	SP211	33.5354°	135.8117°	Granite porphyry	Ring dike	28	9	**15.11**	±	**0.69**	**14**	15.02	±	0.45	9.2
		KUM11	33.8690°	135.9932°	Rhyolite	Lava	55	7	**14.78**	±	**0.25**	**3.5**	14.79	±	0.14	6.2
		IuchiWT	33.8997°	136.1372°	Rhyolitic welded tuff	Welded tuff	57	18	**15.02**	±	**0.16**	**2.5**	14.73	±	0.26	4.3
		KUM16	33.6509°	135.9562°	Granite porphyry	Pluton	80	14	**15.51**	±	**0.41**	**3.5**	15.31	±	0.30	6.8
		KUMA8	34.1076°	136.1770°	Granite porphyry	Pluton	63	33	**14.48**	±	**0.19**	**3.1**	14.61	±	0.20	3.2
		KUMA101	34.1313°	136.1490°	Granite porphyry	Pluton	70	14	**14.76**	±	**0.36**	**5.0**	14.39	±	0.24	4.6
3	Ohmine dike	TKG1	34.0060°	135.8420°	Tuff	Ring dike	52	5	**14.88**	±	**0.45**	**2.5**	15.20	±	0.53	20
4	Shiratani	ST5	34.0056°	135.8909°	Granite	Stock	81	34	**15.60**	±	**0.27**	**2.4**	15.35	±	0.30	3.9
5	Tenguyama	TG2	34.0623°	135.8602°	Granite	Stock	49	17	**15.39**	±	**0.49**	**4.4**	15.07	±	0.42	5.0
6	Kose	KSSP	34.2075°	135.9164°	Granite	Stock	66	23	**14.99**	±	**0.22**	**2.2**	14.98	±	0.21	3.7
7	Shirakura	SK1B	34.2420°	135.9006°	Granodiorite	Stock	40	16	**15.45**	±	**0.28**	**1.5**	15.16	±	0.36	3.8
8	Dorogawa	DO3C	34.2699°	135.9099°	Granodiorite	Stock	25	14	**14.13**	±	**0.29**	**2.0**	14.08	±	0.36	1.9
9	Nakaoku dike	D1	34.3340°	136.0701°	Tuff	Ring dike	70	22	**14.67**	±	**0.24**	**2.9**	14.47	±	0.19	3.4
10	Takamiyama	TA-1	34.4283°	136.0969°	Granite porphyry	Stock	32	11	**13.59**	±	**0.22**	**3.8**	13.48	±	0.48	17
Western Shikoku																
11	Okinoshima	OK1B	32.7410°	132.5453°	Granite	Pluton	55	25	**14.14**	±	**0.18**	**3.1**	14.10	±	0.17	4.2
		OK2C	32.7261°	132.5667°	Granodorite	Pluton	35	11	**14.71**	±	**0.45**	**3.2**	14.50	±	0.36	2.7
12	Kashiwajima	KAS2	32.7731°	132.6399°	Granodorite	Pluton	60	16	**14.99**	±	**0.32**	**2.1**	14.54	±	0.38	3.8
13	Uwajima	UWA1	33.2095°	132.6235°	Granodiorite	Pluton	36	14	**14.93**	±	**0.34**	**3.7**	14.13	±	0.52	4.7
		UWA5	33.2034°	132.6433°	Granodiorite	Pluton	46	20	**15.23**	±	**0.32**	**3.1**	14.87	±	0.39	4.4
		UWA6	33.2006°	132.6454°	Granodiorite	Pluton	50	19	**15.17**	±	**0.29**	**4.0**	14.88	±	0.22	3.2
14	Ishizuchi	EHI38	33.7217°	133.1003°	Granodiorite	Pluton	30	22	**14.35**	±	**0.16**	**1.2**	14.14	±	0.31	2.3
		EHI100	33.7603°	132.9812°	Rhyolitic welded tuff	Welded tuff	30	13	**14.48**	±	**0.16**	**1.12**	14.16	±	0.27	1.6
15	Ishidatami	EHI105	33.6352°	132.6111°	Dacite	Sheet	23	20	**14.37**	±	**0.16**	**3.0**	14.21	±	0.30	4.3
16	Myojin-yama	EHI205	33.7178°	132.7223°	Rhyolite	Sheet	28	17	**14.49**	±	**0.15**	**2.5**	14.49	±	0.22	10.4

Kyushu																	
17	Tanegashima	TQP01	30.4707°	130.8506°	Quartz porphyry	Dike	36	12	**15.48**	±	**0.22**	**1.6**	15.29	±	0.17	3.9
18	Yakushima	YQP01	30.3712°	130.6716°	Quartz porphyry	Dike	36	14	**15.56**	±	**0.28**	**3.4**	Not available			
		YMG16	30.3792°	130.5059°	Granite	Batholith	62	45	**14.71**	±	**0.13**	**1.8**	14.49	±	0.17	2.0
		YKF01	30.3792°	130.5059°	Granite	K-feldspar megacryst	63	24	**14.63**	±	**0.18**	**3.3**	14.47	±	0.15	4.6
		YYG01	30.3347°	130.5059°	Granite	Stock	85	20	**14.60**	±	**0.25**	**2.8**	14.41	±	0.22	4.8
19	Minami–Osumi	OS01	31.3564°	131.0186°	Granodiorite	Batholith	36	11	**14.74**	±	**0.17**	**2.2**	14.83	±	0.22	5.7
20	Takakumayama	TK01	31.4889°	130.7764°	Granite	Stock	27	12	**14.14**	±	**0.31**	**7.1**	14.08	±	0.28	6.4
21	Nomamisaki	SA101A	31.4124°	130.1302°	Granodiorite	Stock	27	12	**14.51**	±	**0.30**	**4.9**	14.44	±	0.23	6.8
22	Kimposan	SA102	31.4747°	130.3770°	Granite	Stock	27	14	**14.32**	±	**0.21**	**1.5**	14.21	±	0.30	2.3
23	Shibisan	SA103	31.9729°	130.3510°	Granite	Stock	27	8	**13.50**	±	**0.15**	**0.97**	13.46	±	0.19	5.9
		SA104	31.9563°	130.3567°	Granite	Stock	28	11	**13.46**	±	**0.30**	**4.0**	13.42	±	0.28	5.3
24	Hioki	SA105	31.6108°	130.3699°	Granite	Stock	27	16	**14.02**	±	**0.23**	**4.9**	14.07	±	0.22	5.1
25	Akanita	SA106	31.5208°	130.4170°	Granite	Stock	36	11	**14.45**	±	**0.26**	**4.0**	14.32	±	0.21	6.5
26	NE Kumagatake	SA107	31.4581°	130.4701°	Granite	Stock	27	13	**14.93**	±	**0.29**	**11.5**	Not available			
27	Osuzuyama	MYA13	32.3418°	131.6173°	Granite porphyry	Sheet or stock	30	8	**14.71**	±	**0.37**	**3.1**	14.63	±	0.31	3.9
28	Murasho	MYA21	32.2295°	131.1601°	Granite porphyry	Dike	30	10	**14.93**	±	**0.26**	**1.9**	14.80	±	0.23	1.7
29	Ichifusayama	IC01	32.3432°	131.0841°	Granite	Stock	36	None of primary magmatic zircon								
		KMJ02	32.3432°	131.0841°	Granite	Stock	45	None of primary magmatic zircon								
30	Okueyama	MYA02	32.7931°	131.2634°	Andesite	Lava	27	17	**14.09**	±	**0.19**	**3.1**	13.94	±	0.18	3.0
		MYA01	32.8028°	131.2668°	Rhyolitic welded tuff	Welded tuff	27	7	**14.00**	±	**0.24**	**0.54**	13.95	±	0.14	1.03
		MYA03	32.7098°	131.4929°	Granite	Stock	32	20	**13.70**	±	**0.13**	**2.0**	13.58	±	0.15	2.7
		MYA05	32.6534°	131.4426°	Granite porphyry	Ring dike	33	13	**14.28**	±	**0.26**	**4.0**	14.17	±	0.20	3.5

*Number of concordant data only includes the primary magmatic zircon population.

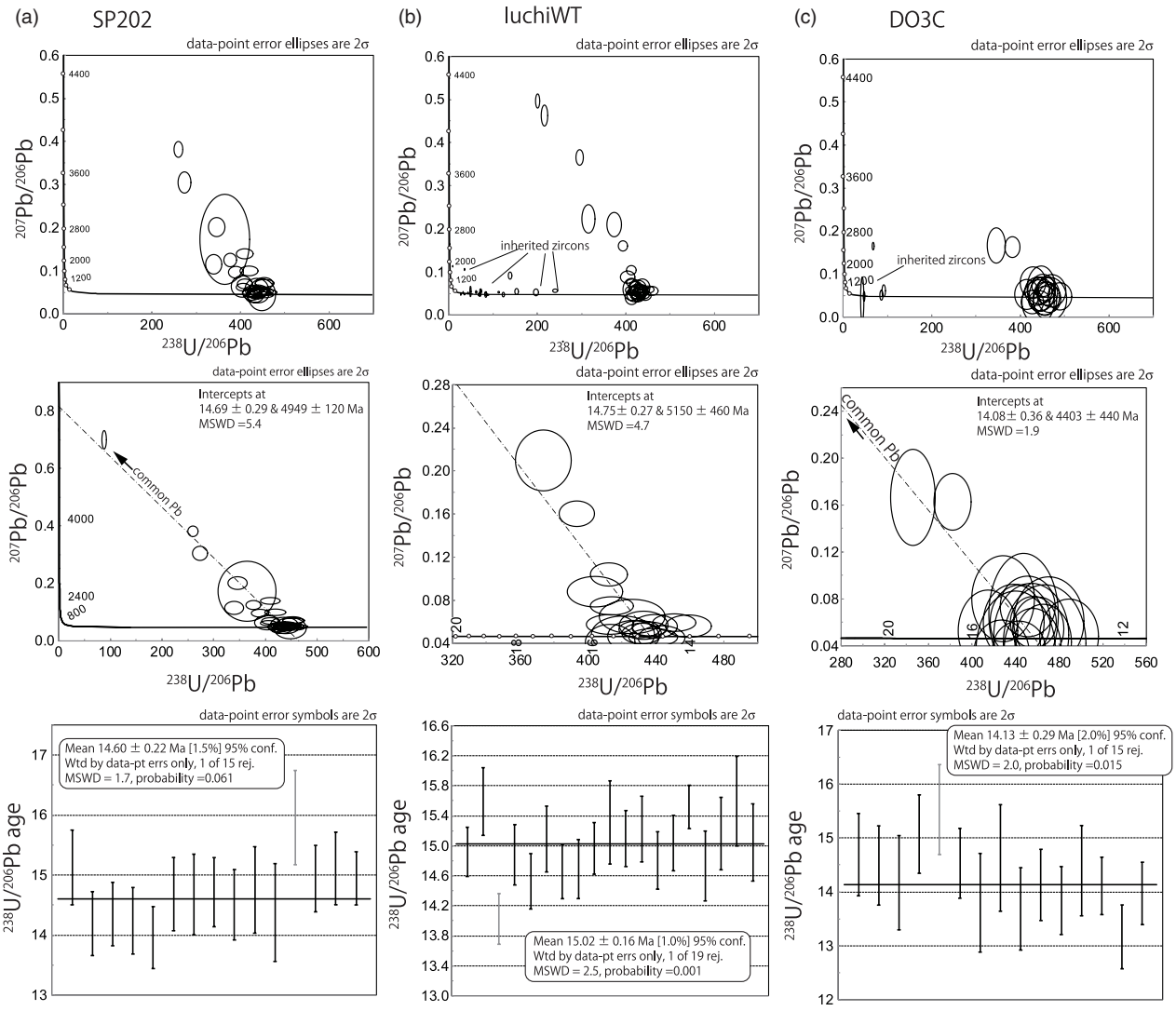

Fig. 9. (a–e) Tera–Wasserburg concordia diagrams and plots of the result of weighted mean calculation of ^{238}U–^{206}Pb ages of concordant primary zircons of five representative samples: (a) Dolerite (SP202) of the Shionomisaki igneous complex in Kii Peninsula; (b) S-type rhyolitic welded tuff (IuchiWT) of the Kumano Acidic Rocks in Kii Peninsula; (c) I-type granodiorite (DO3C) of the Dorogawa pluton in Kii Peninsula; (d) S-type granodiorite (UWA6) of the Uwajima pluton in western Shikoku; (e) I-type granodiorite (EHI38) of Omogo pluton in the Ishizuchi Group, western Shikoku. Tera–Wasserburg diagrams in the second row show the enlarged view including the primary magmatic zircon population together with the regression line to estimate the contamination of common Pb. I-type granitic rocks and dolerite (a, c, e) comprise no or a few inherited zircon grains, and the main cause of discordance is presumed to be common Pb contamination. On the other hand, S-type granitic rocks (b, d) contain a considerable amount of inherited zircon grains in addition to grains affected by common Pb contamination. Grey symbols in the plots of the result of weighted mean calculation show the analysis statistically rejected from the calculation. (f) Concordia diagrams of the zircons from an I-type granodirite (IC01) from Ichifusayama in Kyushu. No primary magmatic zircon was found. The concordia diagram in the second row is the enlarged view of the area younger than 200 Ma. Concordia diagrams and plots of the result of the weighted mean of ^{238}U–^{206}Pb ages of concordant primary zircons for all of the analysed samples are presented in the Supplementary Material (S12) (https://doi.org/10.1017/S0016756819000785).

K–Ar and fission-track dating data with large analytical uncertainties. Hoshi *et al.* (2015*a*) conducted an intensive palaeomagnetic study of the Mizunami Group in the eastern part of the arc, where depositional ages are well constrained by biostratigraphy, and concluded that rapid clockwise rotation began after 17.5 Ma and largely ceased before 15.8 Ma. The latest compilation by Hoshi (2018*a*) concluded that the arc rotated clockwise by ~40° between 18 and 16 Ma. Thus, magmatism in the Outer Zone started immediately after rotation of the SW Japan arc ceased.

Recent radiometric dating of Setouchi Volcanic Rocks, including zircon U–Pb methods, has yielded ages ranging from 15.2 to 13.2 Ma (Tatsumi *et al.* 2010; Shinjoe & Orihashi, 2017). Shinjoe *et al.* (2010) reported zircon U–Pb ages of ~13 Ma for the syenite and alkali granite from the Ashizuri igneous complex in the Marginal Zone (Fig. 12). Recent ^{40}Ar–^{39}Ar dating of the alkali basalt/dolerite dikes in the Ashizuri, Shingu and Tanegashima complexes has yielded ages ranging from 15 to 12 Ma (Shinjoe *et al.* 2018). Our new data indicate that, in both Kii Peninsula and southern Kyushu, the magmatism started at ~15.6 Ma. In sum, high-precision radiometric dating shows that all middle Miocene near-trench igneous activity took place just after the opening of the Japan Sea ceased *c.* 16 Ma.

Since the early suggestion by Nakada & Takahashi (1979), researchers have connected the origin of Miocene fore-arc magmatism to the subduction of hot lithosphere of the Shikoku Basin. Under that scenario, magmatism in the Setouchi Volcanic Belt, including high-Mg andesites, has been ascribed to the interaction of slab melt with mantle peridotite (Furukawa & Tatsumi, 1999;

https://doi.org/10.1017/S0016756819000785 Published online by Cambridge University Press

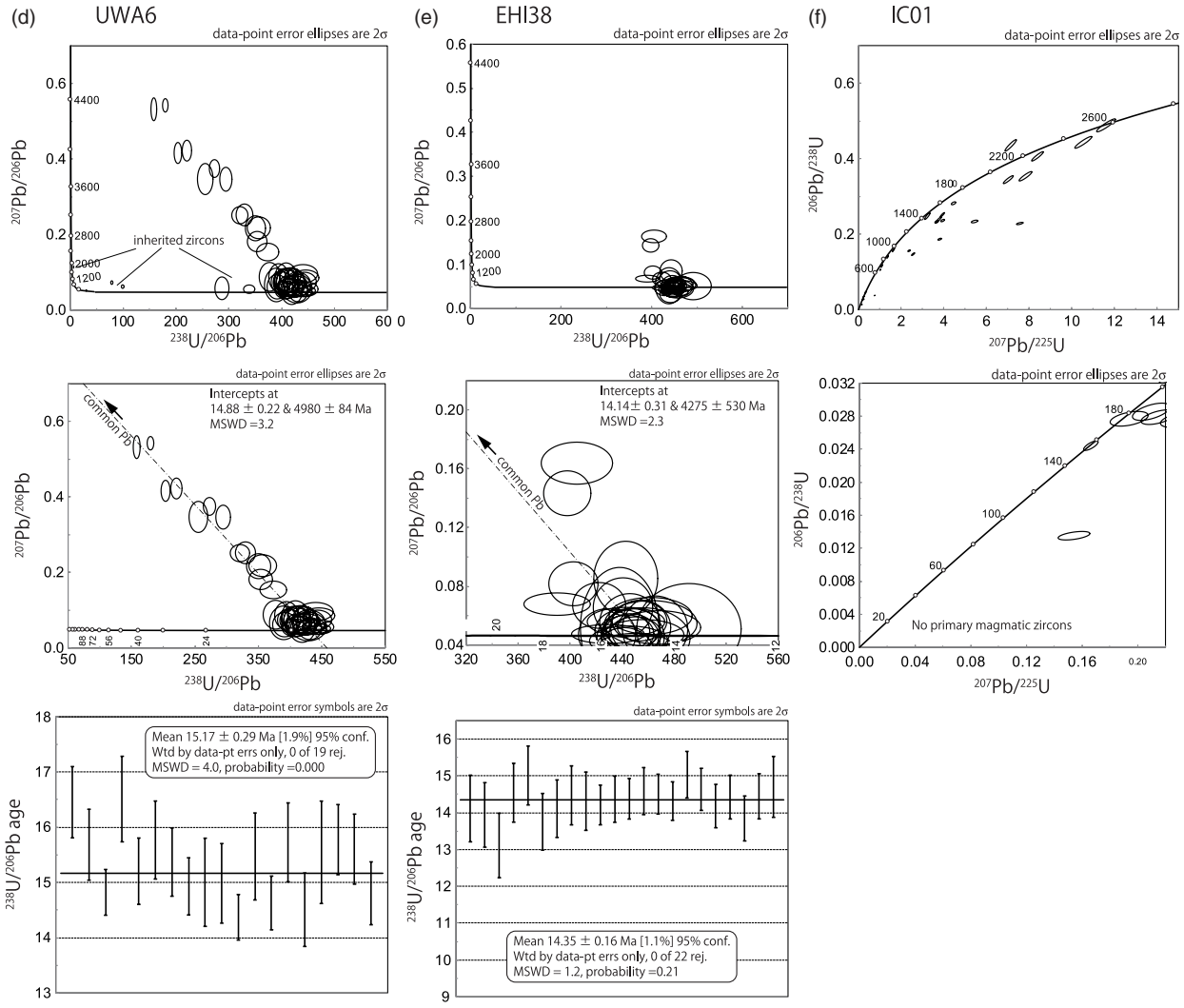

Fig. 9. *(Continued)*

Tatsumi, 2006). The results of this study suggest that Miocene forearc magmatism, in contrast, was connected to the cessation of the opening of the Japan Sea.

Granitic melts that originate by partial melting of subducted slabs and their accompanying sediments may form and rise to shallow levels, as suggested in the Chile Ridge subduction zone where hot oceanic lithosphere is subducted (Anma *et al.* 2009; Anma & Orihashi, 2013; Shin *et al.* 2015), as illustrated in the SW Japan arc during the incipient stage of subduction of the Philippine Sea plate according to structural, petrological and geochronological studies (e.g. Anma, 1997; Anma & Sokoutis, 1997; Anma *et al.* 1998; Kimura *et al.* 2014), and as experimentally demonstrated for subducted sediments (e.g. Patino Douce, 1996) and fluids (Iwamori, 1998, 2000). Such shallow melts or fluids in subduction zones may act as lubricants that decrease friction between the subducting slab and the overriding crust (Anma & Sokoutis, 1997). Thus, it may have been relatively easy for the crust of the SW Japan arc to move southward as the Japan Sea opened. As the melt or fluid escaped, the plate interface between the hot, relatively buoyant subducting lithosphere of the Shikoku Basin and the SW Japan arc crust would have become locked as the lubricating effect decreased. Perhaps the plutons intruding into the SW Japan arc crust across the plate interface contributed to the locking. Together, these resistive mechanisms may have slowed or halted the southward migration of the SW Japan arc crust and the opening of the Japan Sea.

5.b. Philippine Sea plate reconstruction

Reconstructions of the configuration and motion of the Philippine Sea plate must rely largely on palaeomagnetic evidence, because it lacks active spreading zones or hotspot tracks that can be utilized in global plate circuits (Seton *et al.* 2012). Palaeomagnetic studies indicate that the Philippine Sea plate has moved northward by ~20° of latitude and rotated clockwise as much as 110° since Eocene time (e.g. Louden, 1977; Ali & Hall, 1995; Hall *et al.* 1995; Yamazaki *et al.* 2010). Yamazaki *et al.* (2010) presented a model in which the Philippine Sea plate rotated 90° clockwise between 50 and 15 Ma, based on palaeomagnetic data of drilled cores from the Kyushu–Palau Ridge and other localities. Wu *et al.* (2016) noted in their compilation of palaeomagnetic data that the major uncertainty in the rotation of the whole Philippine Sea plate arises from the possibility of local rotation of neighbouring plates or blocks at its margins. Since the early work by Seno & Maruyama (1984), most palaeogeographic reconstructions of the Philippine Sea plate have abandoned the anchored slab model that

https://doi.org/10.1017/S0016756819000785 Published online by Cambridge University Press

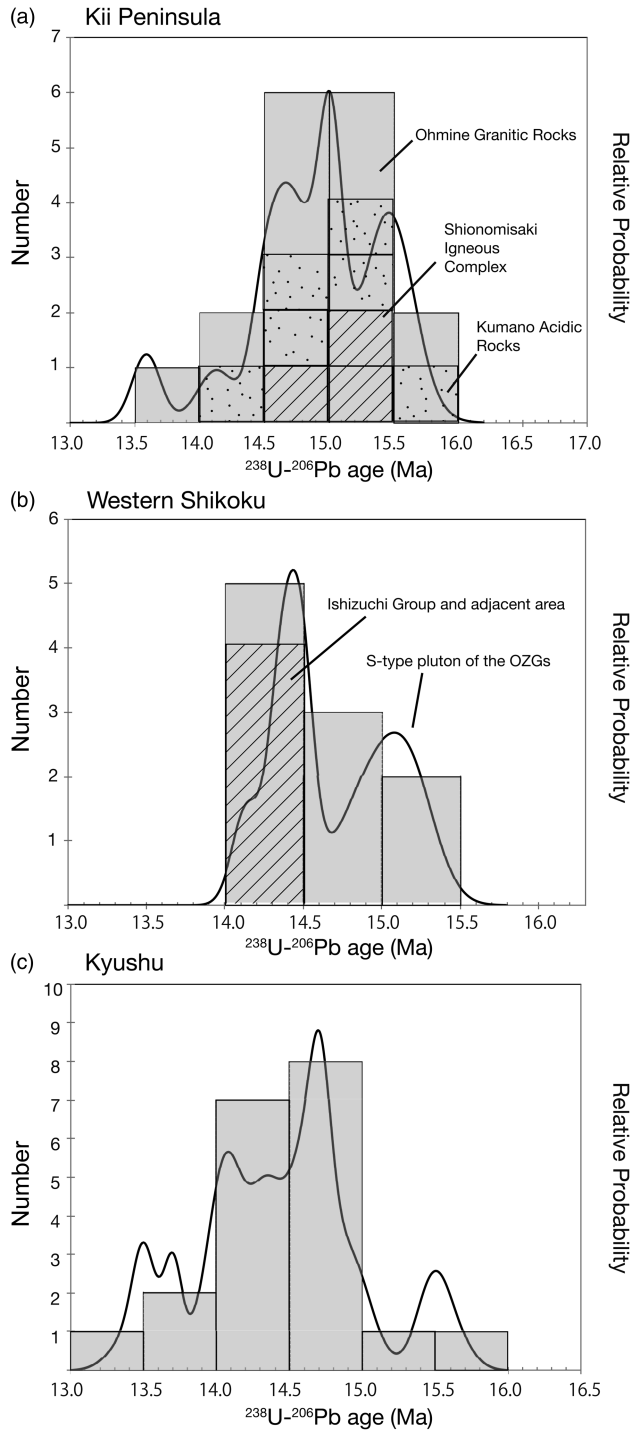

Fig. 10. Probability density plots and histograms of ^{238}U–^{206}Pb ages of the middle Miocene felsic rocks of the SW Japan arc from (a) the Kii Peninsula, (b) western Shikoku and (c) Kyushu.

assumes a fixed plate boundary and adopted a retreating-trench model in which the palaeo-IBM arc migrated along the margin of SW Japan as the Shikoku Basin continued to open. There are two variants of this model, one in which the TTT triple junction migrates early and the other in which it migrates late. Emphasizing the clockwise rotation of the Philippine Sea plate, the late migration model (Fig. 17a) involves the northern end of the palaeo-IBM arc shifting eastward from Kyushu to the Izu Peninsula (its present position) from 15 to 5 Ma (e.g. Hall, 2002; Sdrolias *et al.* 2004; Clift *et al.* 2013). However, Okino (1994) reported that the Shikoku Basin has not rotated significantly since 16 Ma, citing palaeomagnetic data from the Kinan seamount chain in the middle of the Shikoku Basin.

Kimura *et al.* (2014) adopted the late migration model when discussing the origin of near-trench magmatism in the SW Japan arc. They presumed that near-trench magmatism produced its variety of petrological characteristics through the combination of the subduction of the active spreading ridge in the Philippine Sea plate, plus its neighbouring hot lithosphere, and the collision of the palaeo-IBM arc. They cited radiometric ages from the SW Japan arc that indicated eastward younging of near-trench magmatism to account for the contribution from the palaeo-IBM arc. However, most of their data were conventional K–Ar or fission-track ages, which represent cooling ages to ~300 to 250 °C and are subject to significant uncertainty. They also called upon the collision of the palaeo-IBM arc to explain the coastal embayments between capes Ashizurimisaki, Murotomisaki and Shionomisaki. Raimbourg *et al.* (2017) investigated the collision of the palaeo-IBM arc with the SW Japan margin by analysing deformation kinematics and by mapping peak palaeotemperatures through Raman spectra analysis of carbonaceous materials in Cretaceous to Neogene sedimentary rocks of the accretionary Shimanto Supergroup. They claimed that the collision of the palaeo-IBM arc took place in early Miocene time, before near-trench magmatism began in the SW Japan arc. They recognized that the heating event and most of the deformation recorded in the accreted unit occurred in early Miocene time, followed by rapid subsidence and deposition of the fore-arc basin sediments.

An alternative model proposes that a narrow wedge-shaped western extension of the Pacific plate north of the Philippine Sea plate was subducting beneath SW Japan before the Japan Sea opened (Fig. 17b; Hibbard & Karig, 1990). In this model, the Pacific plate extension was consumed as the trench retreated during the rotation of the SW Japan arc, and the Philippine Sea plate started to subduct in turn. Yamaji & Yoshida (1998) proposed that this western extension of the Pacific plate was detached at ~20 Ma to form the Heike plate, which shared a divergent boundary with the Philippine Sea plate (Fig. 17c). As the Heike plate was subducted beneath the SW Japan arc, the hot trench-subparallel spreading ridge between the Heike and Philippine Sea plates was also eventually subducted beneath the SW Japan arc.

Our U–Pb age data from the Outer Zone show that near-trench magmatism started simultaneously over the 600 km distance from the Kii Peninsula to Kyushu at ~15.6 Ma. Thus, the IBM arc must have been east of the Kii Peninsula at 15.6 Ma, given that the magmatism arose from subduction of hot Shikoku Basin lithosphere. Our data clearly do not support late migration models in which the TTT triple junction migrated from Kyushu to the Kii Peninsula after 15 Ma (Fig. 17a).

The Heike plate hypothesis (Fig. 17c) can explain the timing and extent of the near-trench magmatism, though a hypothesis based on a completely vanished microplate may be difficult to test. Moreover, if subduction of a trench-parallel spreading ridge did occur, the young hot oceanic plate adjoining the ridge would have been subducted first. This would have triggered near-trench magmatism in advance of the main pulse of magmatism caused by subduction of the spreading ridge. However, no such precursory magmatism has been found in the study area.

Of all these proposed plate configurations, we favour a model involving subduction of the Pacific plate before the rotation of the

https://doi.org/10.1017/S0016756819000785 Published online by Cambridge University Press

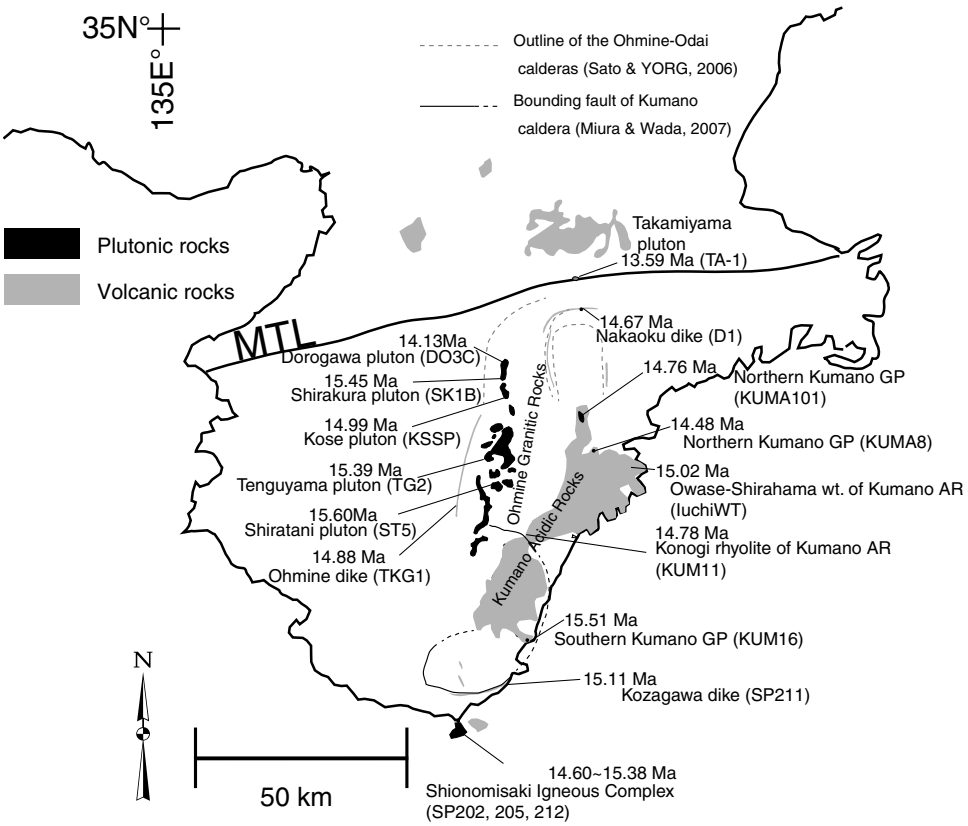

Fig. 11. Outline map of the Kii Peninsula showing the distribution of near-trench igneous rocks and their zircon U–Pb ages. Sample identifications are the same as those listed in Table 3. MTL, Median Tectonic Line.

SW Japan arc (Fig. 17b) because it maintains arc magmatism along the Japanese Islands before the arc began to rotate (Fig. 18a). Wu *et al.* (2016) based their discussion of Philippine Sea plate tectonics on a 3D seismic tomographic model of the subducted slab, which led them to address the Miocene tectonics of the Ryukyu and SW Japan arcs. Their model presumed that the Pacific plate was subducting beneath the SW Japan arc before the arc began its rotation. It also posited that a south-directed subduction zone on the northern edge of the Philippine Sea plate led to the formation of a volcanic arc there, the northern Philippine Sea arc (Fig. 18a). Our model adopts this northern Philippine Sea arc and supposes that it collided with the Ryukyu and SW Japan arcs in middle Miocene time. Although our chronological data cannot directly evaluate the presence of this arc, some geologic evidence in the SW Japan arc margin, such as compressional deformation in the early to middle Miocene Shimanto Belt in Kyushu and Shikoku that is usually interpreted in terms of the late migration model as the result of interactions with the palaeo-IBM arc, may instead be related to the collision of the northern Philippine Sea arc. As the SW Japan arc rotated clockwise, the wedge-shaped extension of the Pacific plate was consumed. Next, the hot Shikoku Basin lithosphere in the Philippine Sea plate began to subduct beneath the SW Japan arc, and widespread near-trench magmatism ensued (Fig. 18b) as the palaeo-IBM arc impinged upon Japan and approached its present position.

The question of when the collision of the palaeo-IBM arc began is a controversial issue (e.g. Kimura *et al.* 2014), and models based on late migration of the TTT triple junction depend on a young (<10 Ma) collision (e.g. Amano, 1991) as supported by geologic evidence such as collision-related conglomerates. However, a recent review of palaeomagnetic evidence has suggested that the Kanto syntaxis, a deformation structure attributed to the collision of the palaeo-IBM arc with Honshu (Fig. 18b), formed early, between 17 and 15 Ma (Hoshi, 2018*b*). This palaeomagnetic argument is consistent with our radiometric age data indicating that the SW Japan arc began to interact with the subducting Philippine Sea plate before 15.6 Ma.

The origin of near-trench magmas in the SW Japan arc is usually ascribed to the subduction of the Shikoku Basin lithosphere and its active spreading ridge (e.g. Kimura *et al.* 2005). Underplating of basaltic magmas from the subducting ridge may have been a heat source for crustal melting in the near-trench region. Additionally, the basaltic magmas may have contributed the mantle-derived component of the felsic magmas that is evident from their Sr–Nd isotopic compositions. Other supporting evidence includes the intrusion of MORB-like tholeiitic basaltic rocks in the Shionomisaki and Murotomisaki igneous bodies near the trench (Section 2.a.3) and the presence of basaltic enclaves in the porphyritic granite of the KARs in the Kii Peninsula (Harada, 1961). However, the trench-normal fossil spreading ridge in the Shikoku Basin (the Kinan seamount chain) is now subducting underneath the Nankai Trough at the position of the channel between the Kii Peninsula and Shikoku (Fig. 1; Okino *et al.* 1999). If subduction of this trench-normal ridge was the major heat source of the near-trench magmatism, the centre of magma production should have followed the position of the subducting ridge as it migrated along the SW Japan arc. One such example is the along-arc progression of Cretaceous granitic rocks in SW Japan evident in K–Ar and Rb–Sr ages (Nakajima *et al.* 1990) and U–Pb ages (Iida *et al.* 2015), which has been ascribed to the subduction of the Kula–Pacific ridge. However, no such trend is apparent in our U–Pb ages for the near-trench Miocene felsic rocks in the SW Japan arc.

https://doi.org/10.1017/S0016756819000785 Published online by Cambridge University Press

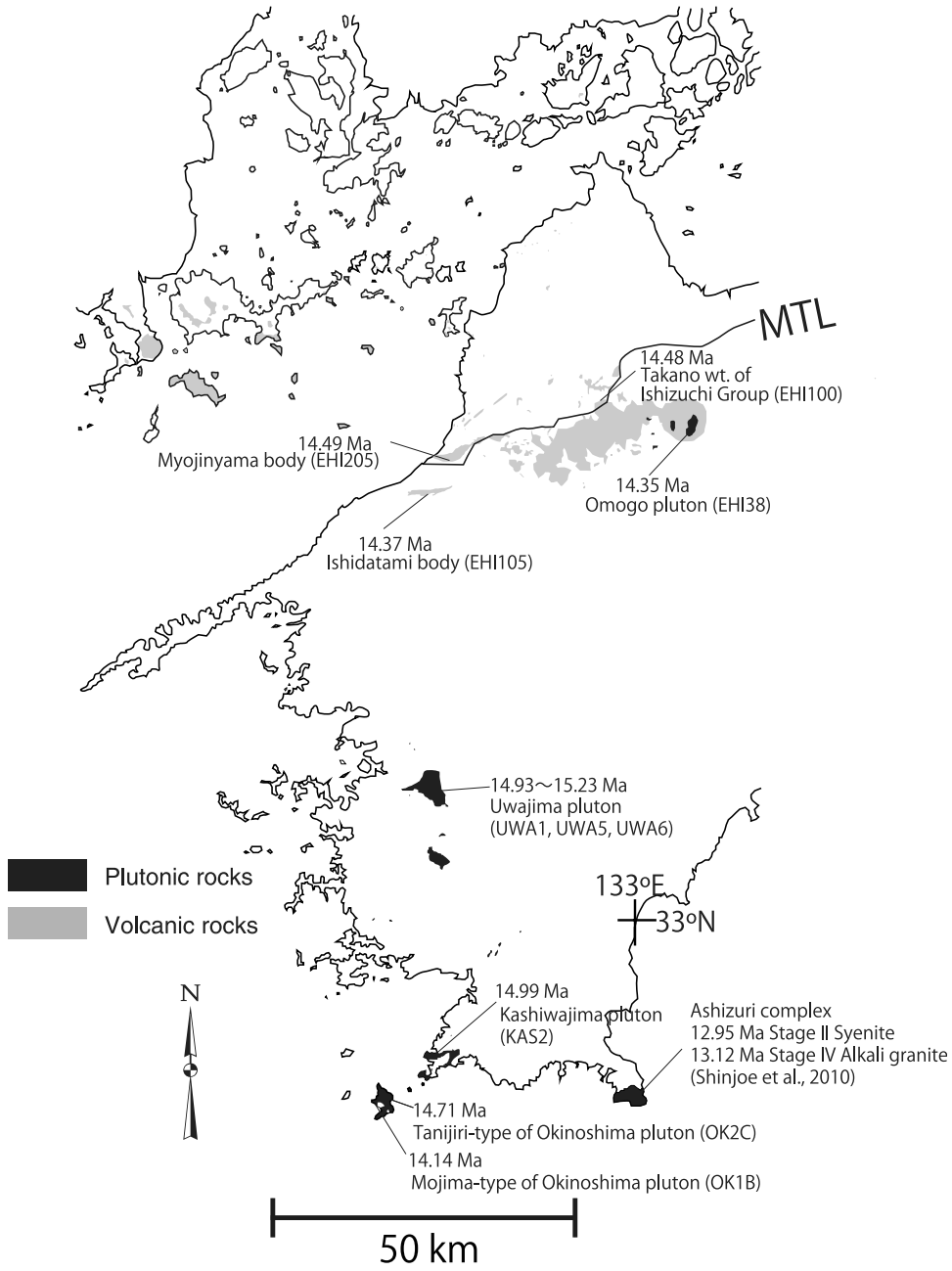

Fig. 12. Outline map of western Shikoku showing the distribution of near-trench igneous rocks and their zircon U–Pb ages. Sample identifications are the same as those listed in Table 3. MTL, Median Tectonic Line. U–Pb zircon ages for the Ashizuri igneous complex are shown for comparison (Shinjoe *et al.* 2010).

The uniformity of magmatism ages along the arc might be explained by segmentation of the Shikoku Basin spreading ridge. Okino *et al.* (1999) showed from the bathymetry and magnetic anomalies of the Philippine Sea plate that this ridge was highly segmented by ~19 Ma, when the ridge's spreading direction changed from E–W to NE–SW. Sets of en echelon ridges meeting at the margin of the SW Japan arc might have supplied heat to a wide region along the arc.

Another explanation for the uniform ages of near-trench magmatism is that the mantle wedge was uniformly hot just after the rotation of the SW Japan arc and formation of the Sea of Japan. Although the primary cause of the back-arc rifting is controversial, back-arc basin formation is accompanied by upwelling of asthenospheric mantle, such that temperatures in the mantle wedge are higher than in subduction zones without back-arc basins (Tatsumi *et al.* 1990). High-Mg andesites are widely found in the Setouchi Volcanic Rocks, distributed north of the Median Tectonic Line just outside the Outer Zone (Fig. 2). Their genesis has been ascribed to the partial melting of subducted Shikoku Basin lithosphere, subsequent melt–mantle interactions, and equilibration with the uppermost mantle (e.g. Shimoda *et al.* 1998; Tatsumi, 2006). Melt production from the hot Shikoku Basin slab probably also occurred in the Outer Zone (Orihashi *et al.* 2000). In areas of the Outer Zone near the trench where bodies of S-type granite predominate, pervasive melting of sediments above the subducting slab must have occurred, as the plate interface is filled with fertile accreted sediments. Metasedimentary xenoliths in the S-type granites record metamorphic conditions

https://doi.org/10.1017/S0016756819000785 Published online by Cambridge University Press

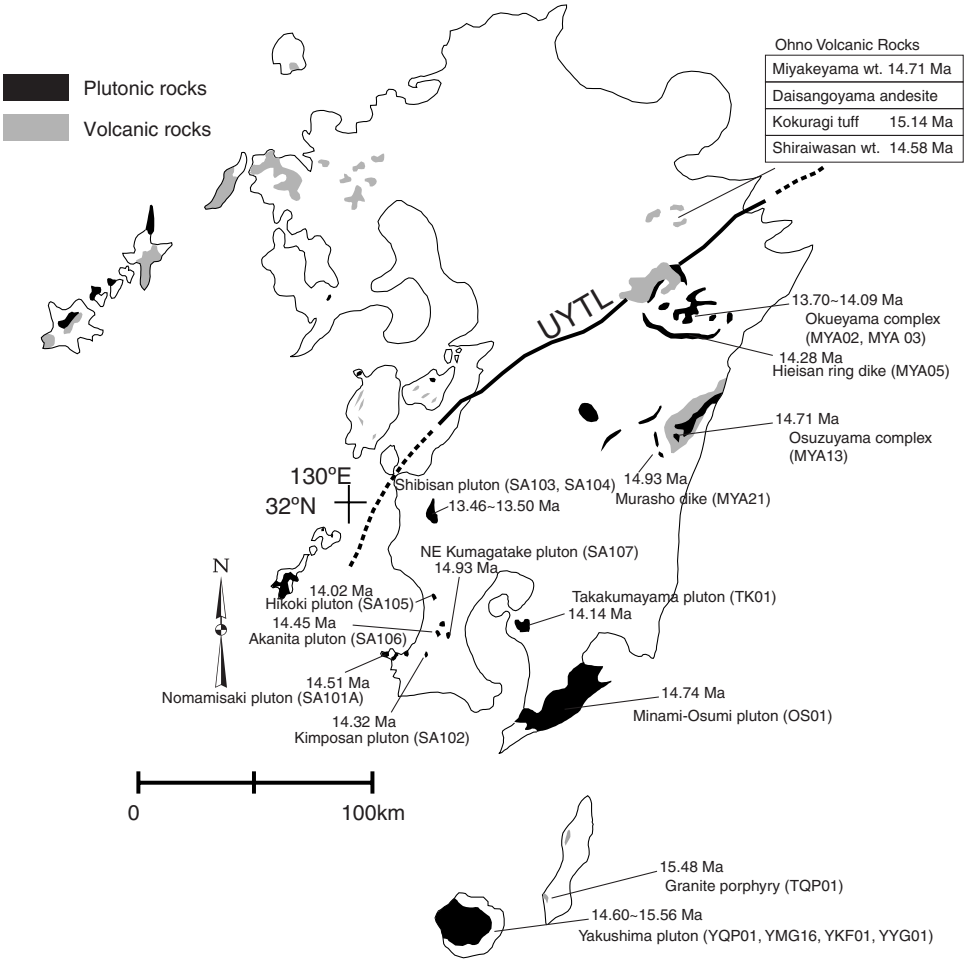

Fig. 13. Outline map of Kyushu showing the distribution of near-trench igneous rocks and their zircon U–Pb ages. UYTL, Usuki–Yatsushiro Tectonic Line. U–Pb zircon ages for the Ohno Volcanic Rocks, a member of the Setouchi Volcanic Rocks, are listed at the top for comparison (Shinjoe & Orihashi, 2017).

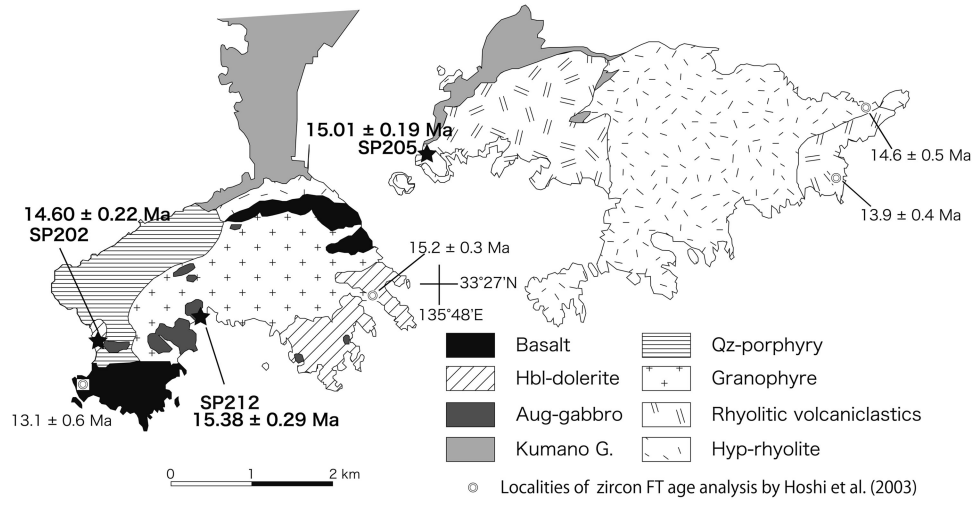

Fig. 14. Lithological map of the Shionomisaki Igneous Complex at the southernmost tip of the Kii Peninsula showing sample localities and U–Pb ages. Zircon fission-track ages (Hoshi *et al.* 2003) and sample locations are shown for comparison.

close to the solidus of sediment and pressures up to 0.74 GPa (Murata, 1984; Shinjoe, 1997) that correspond to the depth of the bottom of the large batholith inferred from a magnetotelluric survey in the Kii Peninsula (Fujita *et al.* 1997; Umeda *et al.* 2003). In the area where OZGs are distributed, the mantle wedge might not have been mature enough for widespread mafic to intermediate magnesian magmas to form via slab melt–mantle reactions. However, enclaves of magnesian andesite to dacite have been sporadically reported from OZGs (Nakada, 1983; Shinjoe, 1997; Shinjoe *et al.* 2005); thus slab melt interacting with mantle wedge peridotite may have contributed a heat source and mantle-derived components to some of the OGRs (Shinjoe, 1997).

https://doi.org/10.1017/S0016756819000785 Published online by Cambridge University Press

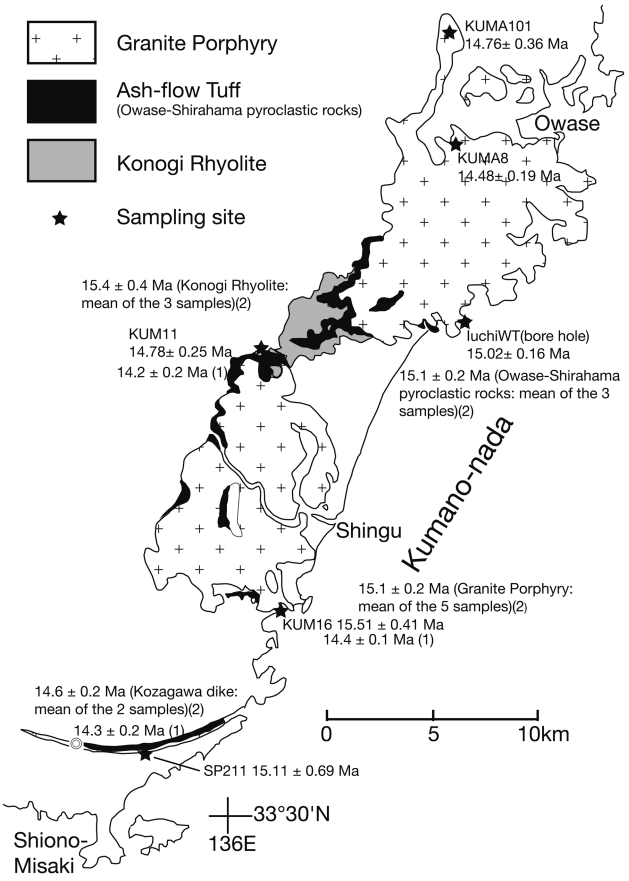

Fig. 15. Lithological map of the Kumano Acidic Rocks in the SE Kii Peninsula showing sample localities and U–Pb ages. Previous dating results are shown for comparison: K–Ar ages are marked '1' (Sumii *et al.* 1998) and zircon fission-track ages are marked '2' (Iwano *et al.* 2007).

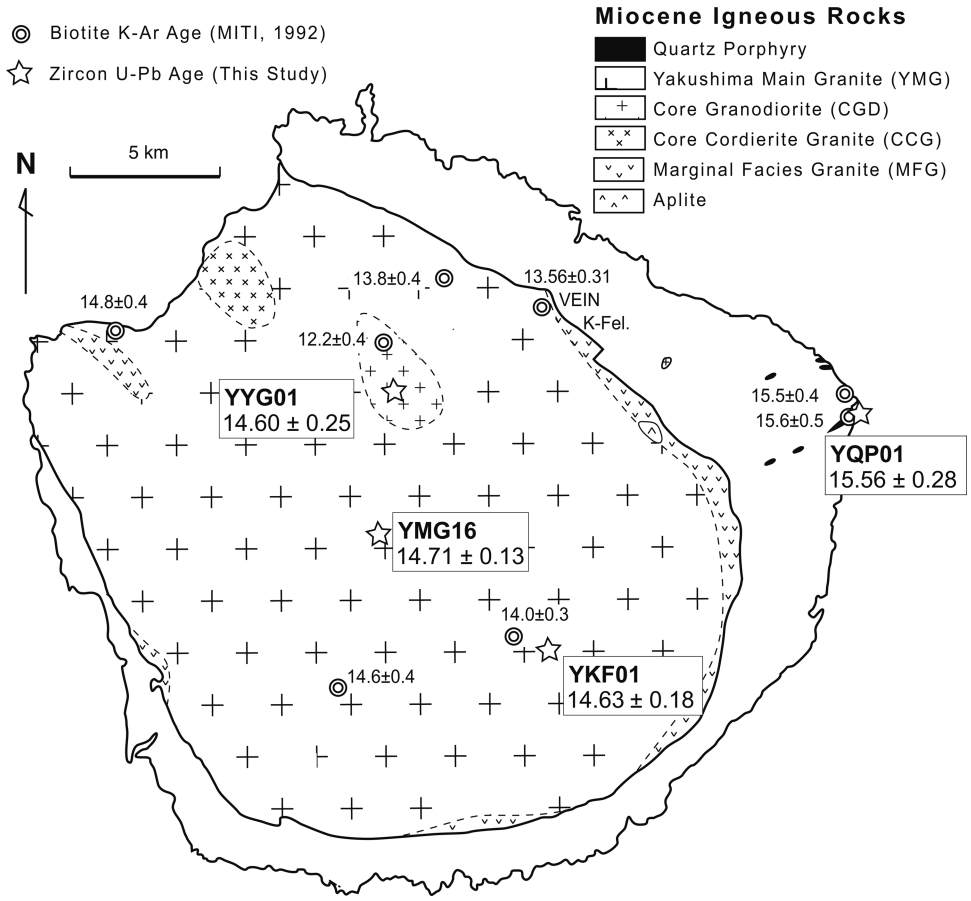

Fig. 16. Lithological map of the Yakushima pluton in Yakushima Island, south of Kyushu, showing sample localities and U–Pb ages. K–Ar ages from MITI (1992) are shown for comparison.

https://doi.org/10.1017/S0016756819000785 Published online by Cambridge University Press

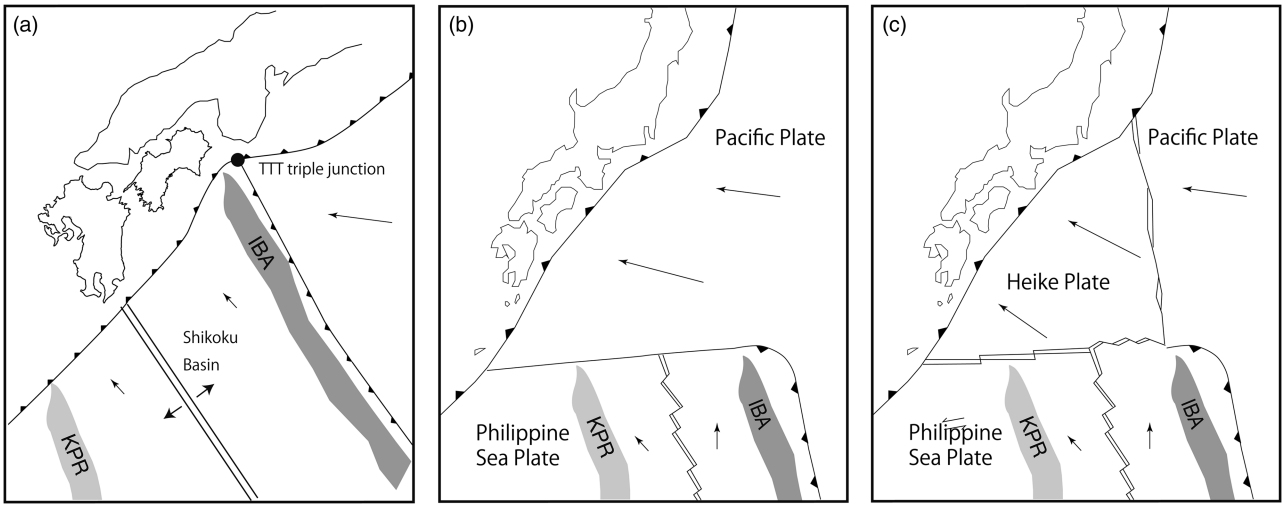

Fig. 17. Miocene plate configuration models around SW Japan. IBA, palaeo-IBM arc; KPR, Kyushu–Palau Ridge. (a) Late TTT triple junction migration model (e.g. Sdrolias *et al.* 2004; Kimura *et al.* 2014). The palaeo-IBM arc migrates along the margin from Kyushu to the Izu Peninsula from 15 to 5 Ma during near-trench magmatism in the SW Japan arc. (b) Plate configuration showing subduction of the Pacific plate before the rapid rotation of SW Japan (e.g. Hibbard & Karig, 1990). (c) Plate configuration based on the Heike plate hypothesis (Yamaji & Yoshida, 1998) before the rapid rotation of SW Japan.

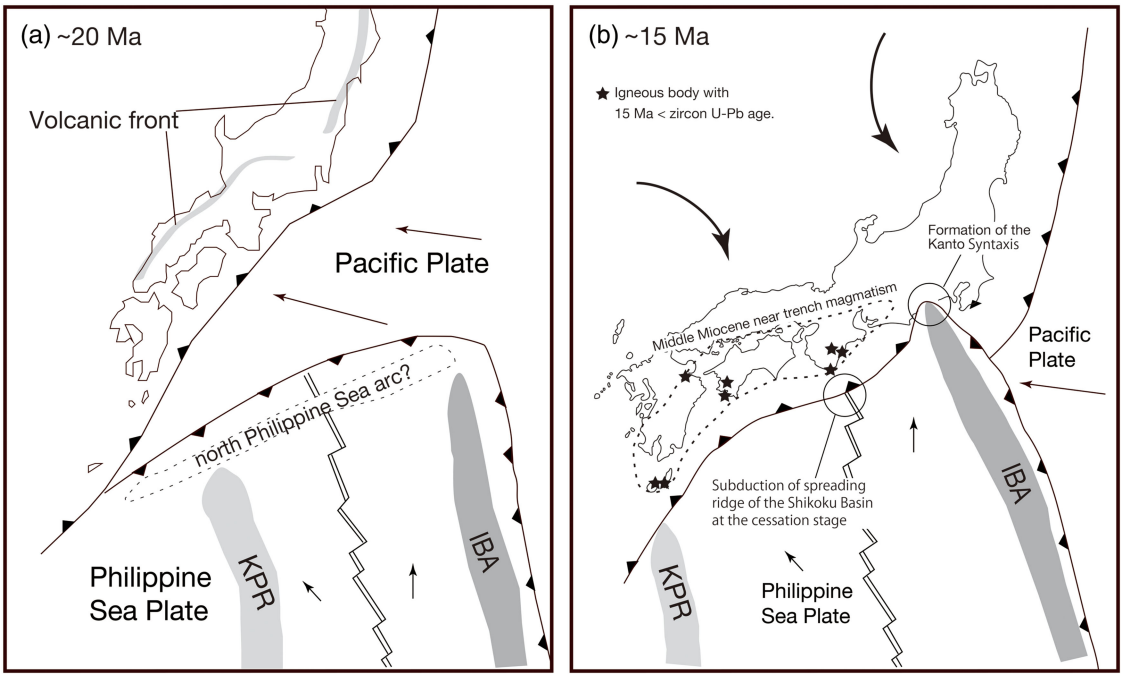

Fig. 18. Plate configuration model of the SW Japan arc in middle Miocene time. (a) At ~20 Ma, before the opening of the Japan Sea and rotation of the SW Japan arc, the Pacific plate subducted beneath the entire length of the Japanese islands and formed a volcanic arc well inboard of the trench (arc position from Kano *et al.* 1991, and Hoshi *et al.* 2015*b*). No magmatism took place near the trench in the SW Japan arc. (b) At ~15 Ma, clockwise rotation of the SW Japan arc led to consumption of the wedge-shaped section of the Pacific plate and hot lithosphere of the Shikoku Basin in the Philippine Sea plate subducted beneath the SW Japan arc to cause near-trench magmatism (black stars) from Kyushu to the Kii Peninsula starting ~15.6 Ma. The simultaneous onset of near-trench magmatism over this part of the trench requires that the palaeo-IBM arc was located east of the Kii Peninsula, where its collision with Honshu formed the Kanto syntaxis before 15 Ma (Hoshi, 2018*b*).

6. Conclusions

Our new dataset of zircon U–Pb ages for the middle Miocene near-trench volcanic and plutonic rocks of the SW Japan arc sheds light on the relationship between igneous activities and the tectonic events of the time, including the opening of the Japan Sea and the migration and early subduction of hot young lithosphere of the Philippine Sea plate. Our major findings are listed below.

1. Precursory magmatism, characterized by dike and stock intrusions, started ~15.6 Ma in both Kyushu and the Kii Peninsula.

https://doi.org/10.1017/S0016756819000785 Published online by Cambridge University Press

2. Most plutonism occurred between 15.5 and 13.5 Ma, in an area 600 km long and 150 km wide.
3. The precursory magmatism ~15.6 Ma occurred in the region closest to the trench. Youngest plutons are distributed in the region further to the trench.
4. No trends are apparent in U–Pb ages along the length of the arc.
5. All of the middle Miocene igneous activity took place shortly after the opening of the Japan Sea ended at *c.* 16 Ma.

From these findings, we argue that the extraction of melts from the slab affected the frictional properties on the plate interface and allowed the overriding crust to migrate. Later emplacement of granite plutons from a relatively buoyant hot slab in the near-trench region may have counteracted this change.

Our data also imply that the TTT triple junction between the Japan and IBM arcs must have reached a position east of the Kii Peninsula by 15.6 Ma, because otherwise a clear younging trend from west to east should have resulted from the migration of the spreading ridge in the Shikoku Basin on the Philippine Sea plate, now fossilized as the Kinan seamount chain.

The widespread contemporaneous magmatic activity along the SW Japan arc requires a wide heat source extending parallel to the trench. Our favoured candidates for this heat source include subduction of a trench-parallel ridge such as that which may have once existed between the extinct Heike plate and the Philippine Sea plate, or subduction of a young and highly segmented ridge system on the Philippine Sea plate, that developed by ~19 Ma as its spreading direction shifted from E–W to NE–SW in addition to the hot wedge mantle condition related to the opening of Japan Sea.

Acknowledgements. This research was financially supported by Grant-in-Aid for Scientific Research from MEXT of Japan (#25400527 and #16K05583), Grant-in-Aid from Fujiwara Natural History Foundation (FY 2014), and the Tokyo Keizai University Research Grant (18-16) to H.S. LA-ICP-MS analyses were supported by the Earthquake Research Institute cooperative research program of the University of Tokyo. A borehole sample of the Kumano Acidic Rocks was kindly provided by Geological Survey of Japan, AIST. We thank Prof. Yutaka Wada (Nara University of Education) for providing a tuffite dike rock sample in Kii Peninsula and field guidance. We also thank Mr Tomoaki Sumii (Geological Survey of Japan, AIST) for guidance in the field of OGRs and KARs and for providing valuable information on the OZGs. We are indebted to Dr Tokomazu Hokada (National Institute of Polar Research) and Dr Masanori Kurosawa (Tsukuba University) for guidance in SEM/CL observations. Revisions by two anonymous referees as well as constructive editorial comments by Professor Yildirim Dilek greatly helped to improve the manuscript.

Supplementary material. To view supplementary material for this article, please visit https://doi.org/10.1017/S0016756819000785.

References

Akatsuka T, Obata M and Yokose H (1999) Formation of layered structure in the Murotomisaki gabbroic complex, especially picrite gabbro, Kochi Prefecture, Japan: quantitative evaluation of crystal accumulation. *Journal of the Geological Society of Japan* **105**, 771–88.

Ali JR and Hall R (1995) Evolution of the boundary between the Philippine Sea plate and Australia: palaeomagnetic evidence from eastern Indonesia. *Tectonophysics* **251**, 251–75. doi: 10.1016/0040-1951(95)00029-1.

Amano K (1991) Multiple collision tectonics of the South Fossa Magna in central Japan. *Modern Geology* **15**, 315–29.

Anderson T (2002) Correction of common lead in U–Pb analyses that do not report ^{204}Pb. *Chemical Geology* **192**, 59–79.

Anma R (1997) Oblique diapirism of the Yakushima Granite in the Ryukyu Arc, Japan. In *Granite: From Segregation of Melt to Emplacement Fabrics* (eds JL Bouchez, DHW Hutton and WE Stephens), pp. 295–318. Dordrecht: Springer.

Anma R, Armstrong R, Orihashi Y, Ike S, Shin K-C, Kon Y, Komiya T, Ota T, Kagashima S, Shibuya T, Yamamoto S, Veloso EE, Fannin M and Herve F (2009) Are the Taitao granites formed due to subduction of the Chile ridge? *Lithos* **113**, 246–58.

Anma R, Kawano Y and Yuhara M (1998) Compositional zoning and its implication in a toroidal circulation inside the Yakushima pluton, SW Japan. *Memoirs of the National Institute of Polar Research* **53**, 157–76.

Anma R and Orihashi Y (2013) Shallow-depth melt eduction due to ridge subduction: LA-ICPMS U-Pb igneous and detrital zircon ages from the Chile Triple Junction and the Taitao Peninsula, Chilean Patagonia. *Geochemical Journal* **47**, 149–65.

Anma R and Sokoutis D (1997) Experimental pluton shapes and tracks above subduction zones. In *Granite: From Segregation of Melt to Emplacement Fabrics* (eds JL Bouchez, DHW Hutton and WE Stephens), pp. 319–34. Dordrecht: Springer.

Aramaki S and Hada S (1965) Geology of the central and southern parts of the Acid Igneous Complex (Kumano Acidic Rocks) in Southeastern Kii Peninsula. *Journal of the Geological Society of Japan* **71**, 494–512.

Clift PD, Carter A, Nicholson U and Masago H (2013) Zircon and apatite thermochronology of the Nankai Trough accretionary prism and trench, Japan: sediment transport in an active and collisional margin setting. *Tectonics* **32**, 377–95.

Dai K, Tsusue A and Honma H (1993) Petrological study of granitic rocks from the Kashiwajima-Okinoshima district in the southwestern part of Kochi Prefecture. *Journal of Mineralogy, Petrology and Economic Geology* **88**, 247–64.

Defant MJ and Drummond MS (1990) Derivation of some modern arc magmas by melting of young subducted lithosphere. *Nature* **347**, 662–5.

DeLong SE, Schwarz WM and Anderson RN (1979) Thermal effects of ridge subduction. *Earth and Planetary Science Letters* **44**, 239–46.

Fujita K, Ogawa Y, Yamaguchi S and Yaskawa K (1997) Magnetotelluric imaging of the SW Japan forearc – a lost paleoland revealed? *Physics of the Earth and Planetary Interiors* **102**, 231–8.

Furukawa Y and Tatsumi Y (1999) Melting of a subducting slab and production of high-Mg andesite magmas: unusual magmatism in SW Japan at 13–15 Ma. *Geophysical Research Letters* **26**, 2271–74.

Geological Survey of Japan (2015) *Seamless Digital Geological Map of Japan 1: 200,000*. 29 May version. Tokyo: Geological Survey of Japan, National Institute of Advanced Industrial Science and Technology.

Hall R (2002) Cenozoic geological and plate tectonic evolution of SE Asia and the SW Pacific: computer-based reconstructions and animations. *Journal of Asian Earth Sciences* **20**, 353–431.

Hall R, Ali JR, Anderson CD and Baker SJ (1995) Origin and motion history of the Philippine sea plate. *Tectonophysics* **251**, 229–50.

Harada K (1961) Some studies on xenoliths from Onigajo, Mie Prefecture. *Journal of the Japanese Association of Mineralogists, Petrologists and Economic Geologists* **45**, 231–38.

Hayashida A and Itoh Y (1984) Paleoposition of Southwest Japan at 16 Ma: implication from paleomagnetism of the Miocene Ichishi Group. *Earth and Planetary Science Letters* **68**, 335–42. doi: 10.1016/0012-821X(84)90164-X.

Hibbard JP and Karig DE (1990) Alternative plate model for the early Miocene evolution of the southwest Japan margin. *Geology* **18**, 170–4.

Hoshi H (2018a) Miocene clockwise rotation of Southwest Japan. *Journal of the Geological Society of Japan* **124**, 675–91.

Hoshi H (2018b) Kanto Syntaxis: when did it begin to grow?. *Journal of the Geological Society of Japan* **124**, 805–17.

Hoshi H, Iwano H, Danhara T and Iwata N (2015b) Dating of altered mafic intrusions by applying a zircon fission track thermochronometer to baked country rock, and implications for the timing of volcanic activity during the opening of the Japan Sea. *Island Arc* **24**, 221–31.

Hoshi H, Iwano H and Yoshida T (2003) Fission-track dating of the Shionomisaki Igneous Complex, Kii Peninsula, Japan. *Journal of the Geological Society of Japan* **109**, 139–50.

Hoshi H, Kamiya N and Kawakami Y (2013) Instantaneous paleomagnetic record from the Miocene Kozagawa Dike of the Kumano Acidic Rocks, Kii Peninsula, Southwest Japan: cautionary note on tectonic interpretation. *Island Arc* **22**, 395–409.

Hoshi H, Kato D, Ando Y and Nakashima K (2015a) Timing of clockwise rotation of Southwest Japan: constraints from new middle Miocene paleomagnetic results. *Earth, Planets and Space* **67**, 92.

Hoshi H and Sano M (2013) Paleomagnetic constraints on Miocene rotation in the central Japan Arc. *Island Arc* **22**, 197–213.

Hoshi H, Tanaka D, Takahashi M and Yoshikawa T (2000) Paleomagnetism of the Nijo Group and its implication for the timing of clockwise rotation of Southwest Japan. *Journal of Mineralogical and Petrological Sciences* **95**, 203–15.

Iida K, Iwamori H, Orihashi Y, Park T, Jwa Y-J, Kwon S-T, Danhara T and Iwano H (2015) Tectonic reconstruction of batholith formation based on the spatiotemporal distribution of Cretaceous–Paleogene granitic rocks in southwestern Japan. *Island Arc* **24**, 205–20.

Ishihara S (1977) The magnetite-series and ilmenite-series granitic rocks. *Mining Geology* **27**, 293–305.

Iwamori H (1998) Transportation of H_2O and melting in subduction zones. *Earth and Planetary Science Letters* **160**, 65–80.

Iwamori H (2000) Thermal effects of ridge subduction and its implications for the origin of granitic batholith and paired metamorphic belts. *Earth and Planetary Science Letters* **181**, 131–44.

Iwano H, Danhara T, Hoshi H, Sumii T, Shinjoe H and Wada Y (2007) Simultaneity and similarity of the Muro Pyroclastic Flow Deposit and the Kumano Acidic Rocks in Kii Peninsula, southwest Japan, based on fission track ages and morphological characteristics of zircon. *Journal of the Geological Society of Japan* **113**, 326–39.

Iwano H, Orihashi Y, Hirata T, Ogasawara M, Danhara T, Horie K, Hasebe N, Sueoka S, Tamura A, Hayasaka Y, Katsube A, Ito H, Tani K, Kimura J, Chang Q, Kouchi Y, Haruta Y and Yamamoto K (2013) An inter-laboratory evaluation of OD-3 zircon for use as a secondary U–Pb dating standard. *Island Arc* **22**, 382–94.

Kano K, Kato H, Yanagisawa Y and Yoshida F (1991) Stratigraphy and geologic history of the Cenozoic of Japan. *Report of the Geological Survey of Japan* **274**.

Kawachi Y and Sato T (1978) Orthoclase megacrysts in the Yakushima granite, southern Kyushu, Japan. *Neues Jahrbuch für Mineralogie – Abhandlungen* **132**, 136–52.

Kawakami Y and Hoshi H (2007) A ring dike and a subhorizontal sheet intrusion in a volcano-plutonic complex: geology of the Kumano Acidic Rocks in the Owase-Kumano area, Kii Peninsula, Japan. *Journal of the Geological Society of Japan* **113**, 296–309.

Kawakami Y, Hoshi H and Yamaguchi Y (2007) Mechanism of caldera collapse and resurgence: observations from the northern part of the Kumano Acidic Rocks, Kii peninsula, southwest Japan. *Journal of Volocanology and Geothermal Research* **167**, 263–81.

Kawano Y, Anma R and Yuhara M (2007) Zoning defined by Sr-isotope initial ratio of the Yakushima granite pluton, Kagoshima. *MAGMA* **88**, 1–16.

Kimura K (1986) Stratigraphy and paleogeography of the Hidakagawa Group of the Northern Shinano Belt in the southern part of Totsugawa Village, Nara Prefecture, Southwest Japan. *Journal of the Geological Society of Japan* **92**, 185–203.

Kimura G, Hashimoto Y, Kitamura Y, Yamaguchi A and Koge H (2014) Middle Miocene swift migration of the TTT triple junction and rapid crustal growth in southwest Japan: a review. *Tectonics* **33**, 1219–38. doi: 10.1002/2014TC003531.

Kimura J-I, Stern RJ and Yoshida T (2005) Reinitiation of subduction and magmatic responses in SW Japan during Neogene time. *Bulletin of Geological Society of America* **117**, 969–86. doi: 10.1130/B25565.1.

Kitagawa Y, Takahashi M, Koizumi N, Mizuochi Y, Murase A and Kawanishi S (2009) *Geological Data of the GSJ Boring Core at the Ichiura Observation Station*. 1 CD-ROM. Tsukuba: Geological Survey of Japan, AIST. GSJ Openfile Report no. 510.

Louden KE (1977) Paleomagnetism of DSDP sediments, phase shifting of magnetic anomalies, and rotations of the West Philippine Basin. *Journal of Geophysical Research* **82**, 2989–3002. doi: 10.1029/JB082i020p02989.

Ludwig KR (2012) *User's Manual for Isoplot 3.75: A Geochronological Toolkit for Microsoft Excel*. Berkeley, CA: Berkeley Geochronology Center, Special Publication no. 5, 75 pp.

Lukács R, Harangi S, Bachmann O, Guillong M, Danišík M, Buret Y, Quadt A, Dunkl I, Fodor L, Sliwinski J, Soós I and Szepesi J (2015) Zircon geochronology and geochemistry to constrain the youngest eruption events and magma evolution of the Mid-Miocene ignimbrite flare-up in the Pannonian Basin, eastern central Europe. *Contributions to Mineralogy and Petrology* **170**, 1–26.

Marshak RS and Karig DE (1977) Triple junctions as a cause for anomalously near-trench igneous activity between the trench and volcanic arc. *Geology* **5**, 233–6.

Maruyama S (1997) Pacific-type orogeny revisited: Miyashiro-type orogeny proposed. *Island Arc* **6**, 91–120.

MITI (Ministry of International Trade and Industry) (1985) *Report of Regional Geological Structure Survey 'Nansatu' Area*. Tokyo: Ministry of International Trade and Industry, 180 pp.

MITI (Ministry of International Trade and Industry) (1992) *Report of Potential Investigation of Rare Metal Mineral Resources: The Yakushima Area, 1991*. Tokyo: Ministry of International Trade and Industry, 171 pp.

Miura D (1999) Arcuate pyroclastic conduits, ring faults, and coherent floor at Kumano caldera, Southwest Honshu, Japan. *Journal of Volcanology and Geothermal Research* **92**, 271–94.

Miura D and Wada Y (2007) Effects of stress in the evolution of large silicic magmatic systems: an example from the Miocene felsic volcanic field at Kii Peninsula, SW Honshu, Japan. *Journal of Volcanology and Geothermal Research* **167**, 300–19.

Miyake Y (1985) MORB-like tholeiites formed within the Miocene forearc basin, Southwest Japan. *Lithos* **18**, 23–34.

Miyazaki K, Ozaki M, Saito M and Toshimitsu S (2016) 2e The Kyushu-Ryukyu Arc. In *Geology of Japan* (eds T Moreno, SR Wallis, T Kojima and W Gibbons), pp. 139–74. London: Geological Society of London.

Mizuno A (1957) *Explanatory Text of the Geological Map of Japan, Scale 1:50,000, Nachi*. Tokyo: Geological Survey of Japan, 37 pp.

Murakami N, Imaoka T and Uozumi S (1989) Ring complex of the Cape of Ashizuri, and its mode of emplacement, Kochi prefecture, Southwest Japan. *Monograph of the Association for the Geological Collaboration in Japan* **36**, 115–42.

Murata M (1982) S-type and I-type granitic rocks of the Ohmine district, central Kii peninsula. *Journal of the Japanese Association of Mineralogists, Petrologists and Economic Geologists* **77**, 267–77.

Murata M (1984) Petrology of Miocene I-type and S-type granitic rocks in the Ohmine district, central Kii peninsula. *Journal of the Japanese Association of Mineralogists, Petrologists and Economic Geologists* **79**, 351–69.

Murata M and Yoshida T (1985) Trace elements behavior in Miocene I-type and S-type granitic rocks in the Ohmine district, central Kii peninsula. *Journal of the Japanese Association of Mineralogists, Petrologists and Economic Geologists* **80**, 227–45.

Nakada S (1983) Zoned magma chamber of the Osuzuyama Acid Rocks, Southwest Japan. *Journal of Petrology* **24**, 471–94.

Nakada S and Takahashi M (1979) Regional variation in chemistry of the Miocene intermediate to felsic magmas in the Outer Zone and the Setouchi Province of Southwest Japan. *Journal of the Geological Society of Japan* **85**, 571–82.

Nakajima T, Sawada Y, Nakagawa T, Hayashi A and Itaya T (1990) Paleomagnetic results and K-Ar dating on Miocene rocks in the northern part of Fukui Prefecture, Central Japan. *Journal of Mineralogy, Petrology and Economic Geology* **85**, 45–59.

Ogasawara M (1997) K-Ar age and geochemical characteristics of the quartz-porphyry at Shimama, southern Tanegashima, and K-Ar age of a lamprophyre from northern Tanegashima: implications for Miocene igneous activities in the Outer Zone of Southwest Japan. *Journal of Mineralogy, Petrology and Economic Geology* **92**, 454–64.

Oikawa T, Umeda K, Kanazawa S and Matsuzaki T (2006) Unusual cooling of the Middle Miocene Ichifusayama Granodiorite, Kyushu, Japan. *Journal of Mineralogical and Petrological Sciences* **101**, 23–8.

Okino K (1994) Evolution of the Shikoku Basin. *Journal of Geomagnetism and Geoelectricity* **46**, 463–79.

Okino K, Ohara Y, Kasuga S and Kato Y (1999) The Philippine Sea: new survey results reveal the structure and the history of the marginal basins. *Geophysical Research Letters* **26**, 2287–90.

Orihashi Y, Inagaki K, Hirata T, Anma R and Hirata D (2000) Zircon REE composition and magma genesis of the Middle Miocene granitic rocks in the Outer Zone of Southwest Japan: on the possibility of slab melting. *Chikyu Monthly Special* **30**, 14–21.

Orihashi Y, Nakai S and Hirata T (2008) U-Pb age determinations for seven standard zircons by ICP-Mass Spectrometry coupled with frequency quintupled Nd-YAG (λ = 213 nm) laser ablation system: comparison with LA-ICP-MS zircon analyses with a NIST glass reference material. *Resource Geology* **58**, 101–23.

Otofuji Y, Itaya T and Matsuda T (1991) Rapid rotation of southwest Japan: palaeomagnetism and K-Ar ages of Miocene volcanic rocks of southwest Japan. *Geophysical Journal International* **105**, 397–405. doi: 10.1111/j.1365-246X.1991.tb06721.x.

Otofuji Y and Matsuda T (1983) Paleomagnetic evidence for the clockwise rotation of Southwest Japan. *Earth and Planetary Science Letters* **62**, 349–59. doi: 10.1016/0012-821x(83)90005-5.

Otofuji Y and Matsuda T (1987) Amount of clockwise rotation of Southwest Japan: fan shape opening of the southwestern part of the Japan Sea. *Earth and Planetary Science Letters* **85**, 289–301. doi: 10.1016/0012-821x(87)90039-2.

Patino Douce AE (1996) Effects of pressure and H_2O content on the compositions of primary crustal melts. *Transactions of the Royal Society of Edinburgh: Earth Science* **87**, 11–21.

Pearce JA, Harris NBW and Tindle AG (1984) Trace element discrimination diagrams for the tectonic interpretation of granitic rocks. *Journal of Petrology* **25**, 956–83.

Raimbourg H, Famin V, Palazzin G, Yamaguchi A and Augier R (2017) Tertiary evolution of the Shimanto belt (Japan): a large-scale collision in Early Miocene. *Tectonics* **36**, 1317–37.

Sato T and Yamato Omine Research Group (YORG) (2006) Omine and Odai cauldrons: arcuate and semicircular faults, dike swarms and collapse structure in the central area of the Kii Mountains, Southwest Japan. *Earth Science (Chikyu Kagaku)* **60**, 403–13.

Sawada Y, Mishiro Y, Imaoka T, Yoshida K, Inada R, Hisai K, Kondo H and Hyodo M (2013) K-Ar ages and paleomagnetism of the Miocene in the Izumo Basin, Shimane Prefecture. *Journal of the Geological Society of Japan* **119**, 267–84.

Sdrolias M, Roest WR and Müller RD (2004) An expression of Philippine Sea plate rotation: the Parece Vela and Shikoku Basins. *Tectonophysics* **394**, 69–86.

Seno T and Maruyama S (1984) Paleogeographic reconstruction and origin of the Philippine Sea. *Tectonophysics* **102**, 53–84.

Seton M, Müller RD, Zahirovic S, Gaina C, Torsvik T, Shephard G, Talsma A, Gurnis M, Turner M, Maus S and Chandler M (2012) Global continental and ocean basin reconstructions since 200 Ma. *Earth-Science Reviews* **113**, 212–70.

Shibata K (1978) Contemporaneity of Tertiary granites in the Outer Zone of Southwest Japan. *Bulletin of the Geological Survey of Japan* **29**, 551–4.

Shibata K and Nozawa T (1967) K-Ar ages of granitic rocks from the Outer Zone of southwest Japan. *Geochemical Journal* **1**, 131–7.

Shimoda G and Tatsumi Y (1999) Generation of rhyolite magmas by melting of subducting sediments in Shodo-Shima island, Southwest Japan, and its bearing on the origin of high-Mg andesites. *Island Arc* **8**, 383–92.

Shimoda G, Tatsumi Y, Nohda S, Ishizaka K and Jahn BM (1998) Setouchi high-Mg andesites revisited: geochemical evidence for melting of subducting sediments. *Earth and Planetary Science Letters* **160**, 479–92.

Shin K-C, Anma R, Nakano T, Orihashi Y and Ike S (2015) The Taitao ophiolite-granite complex, Chile: emplacement of ridge-trench intersection oceanic lithosphere on land and origin of calc-alkaline I-type granites. *Episodes* **38**, 285–99.

Shinjoe H (1997) Origin of the granodiorite in the forearc region of southwest Japan: melting of the Shimanto accretionary prism. *Chemical Geology* **134**, 237–55.

Shinjoe H and Orihashi Y (2017) Zircon U-Pb ages of Ohno volcanic rocks in eastern Kyushu. *Journal of the Geological Society of Japan* **123**, 423–31.

Shinjoe H, Orihashi Y and Sumii T (2010) U-Pb zircon ages of syenitic and granitic rocks in the Ashizuri igneous complex, southwestern Shikoku: constraint for the origin of forearc alkaline magmatism. *Geochemical Journal* **44**, 275–83.

Shinjoe H, Orihashi Y, Wada Y, Sumii T and Nakai S (2007) Regional variation of whole rock chemistry of the Miocene felsic igneous rocks in the Kii Peninsula, southwest Japan. *Journal of the Geological Society of Japan* **113**, 310–25.

Shinjoe H, Shibata T, Yoshikawa M, Orihashi Y and Sudo M (2018) Near-trench alkaline basaltic magmatism in Miocene SW Japan. *Goldschmidt Abstracts*. https://goldschmidtabstracts.info/2018/2331.pdf.

Shinjoe H, Shimoda G, Fukuoka T and Sumii T (2005) Magnesian igneous enclave in the Ohmine Granitic Rocks of Kii Peninsula. *Japanese Magazine of Mineralogical and Petrological Sciences* **34**, 15–23.

Shinjoe H and Sumii T (2001) Catalog of the Middle Miocene igneous rocks in the forearc region of the Southwest Japan: (2) Shikoku district. *Memoir of Human and Natural Sciences, Tokyo Keizai University* **112**, 51–91.

Shinjoe H and Sumii T (2003) Catalog of the Middle Miocene igneous rocks in the forearc region of the Southwest Japan: (2) Kyushu district. *Memoir of Human and Natural Sciences, Tokyo Keizai University* **115**, 31–71.

Stacey JS and Kramers JD (1975) Approximation of terrestrial lead isotope evolution by a two-stage model. *Earth and Planetary Science Letters* **26**, 207–21.

Sumii T (2000) K-A ranges of the Miocene granites in the Takatsuki-yama and the surrounding areas, southwestern Shikoku. *Japanese Magazine of Mineralogical and Petrological Sciences* **29**, 67–73.

Sumii T, Uchiumi S, Shinjoe H and Shimoda G (1998) Re-examination on K-Ar age of the Kumano Acidic Rocks in Kii Peninsula, Southwest Japan. *Journal of the Geological Society of Japan* **104**, 387–94.

Sun S-S and McDonough WF (1989) Chemical and isotopic systematics of oceanic basalts: implications for mantle composition and processes. In *Magmatism in the Ocean Basins* (eds D Saunders and MJ Norry), pp. 313–45. Geological Society of London, Special Publication no. 42.

Taira A (1988) The Shimanto belt in Shikoku, Japan: evolution of Cretaceous to Miocene accretionary prism. *Modern Geology* **12**, 5–46.

Takahashi M (1986a) Anatomy of a middle Miocene valley-type caldera cluster: geology of the Okueyama volcano-plutonic complex, southwest Japan. *Journal of Volcanology and Geothermal Research* **29**, 33–70.

Takahashi M (1986b) Arc magmatism before and after the Japan Sea opening. In *Development of the Japanese Islands: History As a Mobile Belt and the Present State* (eds A Taira and K Nakamura), pp. 218–26. Tokyo: Iwanami Shoten.

Takahashi M, Aramaki S and Ishihara S (1980) Magnetite-series/ilmenite-series vs. I-type/S-type granitoids. *Mining Geology* **8**, 13–28.

Takahashi M, Tono K and Kanamaru T (2014) Whole-rock major element chemistry for igneous rocks of the Okueyama Volcano-plutonic Complex, Kyushu, Southwest Japan: summary of 271 analytical data. *Proceedings of the Institute of Natural Sciences Nihon University* **49**, 173–95.

Takehara M, Horie K, Tani K, Yoshida T, Hokada T and Kiyokawa S (2017) Timescale of magma chamber processes revealed by U–Pb ages, trace element contents and morphology of zircons from the Ishizuchi caldera, Southwest Japan Arc. *Island Arc* **26**, e12182. doi: 10.1111/iar.12182.

Taneda S and Kinoshita K (1972) An Alkaline Rock Body in Tanegashima Island, South Kyushu, Japan. *Bulletin of the Volcanological Society of Japan* **17**, 88–97.

Tatsumi Y (1989) Migration of fluid phases and genesis of basalt magmas in subduction zones. *Journal of Geophysical Research* **94**, 4697–707.

Tatsumi Y (2006) High-Mg andesites in the Setouchi Volcanic Belt, Southwestern Japan: analogy to Archean magmatism and continental crust formation? *Annual Review of Earth and Planetary Science* **34**, 467–99.

Tatsumi Y, Maruyama S and Nohda S (1990) Mechanism of backarc opening in the Japan Sea: role of asthenospheric injection. *Tectonophysics* **181**, 299–306.

Tatsumi Y, Tani K, Sato K, Danhara T, Hyodo H, Kawabata H, Hanyu T and Dunkley DJ (2010) Multi-chronology of volcanic rocks leading to reliable

https://doi.org/10.1017/S0016756819000785 Published online by Cambridge University Press

age estimates of volcanic activity: an example from the Setouchi volcanic rocks on Shodo-Shima Island, SW Japan. *Journal of the Geological Society of Japan* **116**, 661–79.

Tazaki K, Kagami H, Itaya T and Nagao T (1993) K-Ar ages and the origin of acidic volcanic rocks along the Median Tectonic Line at northwest Shikoku, Japan. *Memoir of the Geological Society of Japan* **42**, 267–78.

Terakado Y, Shimizu H and Masuda A (1988) Nd and Sr isotopic variations in acidic rocks formed under a peculiar tectonic environment in Miocene Southwest Japan. *Contributions to Mineralogy and Petrology* **99**, 1–10.

Umeda K, Uehara D, Ogawa Y, Kudo T and Kakuta C (2003) Deep structure of the Miocene Igneous Complex in the Kii Peninsula, southwest Japan, inferred from wide-band magnetotelluric soundings. *Bulletin of Volcanological Society of Japan* **48**, 461–70.

Uto K, Hirai H, Goto K and Arai S (1987) K-Ar ages of carbonate- and mantle nodule-bearing lamprophyre dikes from Shingu, central Shikoku, Southwest Japan. *Geochemical Journal* **21**, 283–90.

Wada Y and Araki M (1997) Takamiyama Acidic Rock: a S-type granitic rock on the Median Tectonic Line, Central Kii Peninsula, Southwest Japan. *Bulletin of Nara University of Education* **46**, 1–15.

Wada Y and Iwano H (2001) Pyroclastic (Tuffite) dikes at Kawakami in Nara prefecture, central Kii Peninsula, SW Japan. *Bulletin of the Volcanological Society of Japan* **46**, 107–15.

Wiedenbeck M, Alle P, Corfu F, Griffin WL, Meier M, Oberli F, Von Quadt A, Roddick JC and Spiegel W (1995) Three natural zircon standards for U-Th-Pb, Lu-Hf, trace element and REE analyses. *Geostandars Newsletter* **19**, 1–23.

Wu J, Suppe J, Lu R and Kanda R (2016) Philippine Sea and East Asian plate tectonics since 52 Ma constrained by new subducted slab reconstruction methods. *Journal of Geophysical Research* **121**, 4670–741. doi: 10.1002/2016JB012923.

Yamaji A and Yoshida T (1998) Multiple tectonic events in the Miocene Japan arc: the Heike microplate hypothesis. *Journal of Mineralogy, Petrology and Economic Geology* **98**, 389–408.

Yamazaki T, Takahashi M, Iryu Y, Sato T, Oda M, Takayanagi H, Chiyonobu S, Nishimura A, Nakazawa T and Ooka T (2010) Philippine Sea Plate motion since the Eocene estimated from paleomagnetism of seafloor drill cores and gravity cores. *Earth Planets Space* **62**, 495–502. doi: 10.5047/eps.2010.04.001.

Yoshida T (1984) Tertiary Ishizuchi Cauldron, Southwest Japan Arc: formation by ring fracture subsidence. *Journal of Geophysical Research* **89**, 8502–10.

https://doi.org/10.1017/S0016756819000785 Published online by Cambridge University Press